THERMOTROPIC LIQUID CRYSTAL MODELS WITH MULTICRITICAL POINTS

Gabriel Krzyzanowski

Dissertação de Mestrado apresentada ao Programa de Pós-graduação em Física Aplicada, PPGFISA, da Universidade Federal da Integração Latino Americana, como parte dos requisitos necessários à obtenção do título de Mestre em Física Aplicada.

Orientador: Dr. Eduardo do Carmo

Foz do Iguaçu
Março de 2026

THERMOTROPIC LIQUID CRYSTAL MODELS WITH MULTICRITICAL POINTS

Gabriel Krzyzanowski

DISSERTAÇÃO SUBMETIDA AO CORPO DOCENTE DO PROGRAMA DE PÓS-GRADUAÇÃO EM FÍSICA APLICADA DA UNIVERSIDADE FEDERAL DE INTEGRAÇÃO LATINO AMERICANA COMO PARTE DOS REQUISITOS NECESSÁRIOS PARA A OBTENÇÃO DO GRAU DE MESTRE EM CIÊNCIAS EM FÍSICA APLICADA.

Orientador: Dr. Eduardo do Carmo

Comissão Examinadora: Prof. Dr. André de Pinho Vieira
Prof. Dr. Luciano Calheiros Lapas

FOZ DO IGUAÇU, PR – BRASIL
MARÇO DE 2026

Catalogação elaborada pelo Setor de Tratamento da Informação
Catalogação de Publicação na Fonte. UNILA - BIBLIOTECA LATINO-AMERICANA - CENTRAL

A447
Almeida, Gabriel Krzyzanowski de.
Thermotropic liquid crystal models with multicritical points / Gabriel Krzyzanowski de Almeida. - Foz do Iguaçu, 2026.
52 f.: il.

Dissertação (Mestrado) - Universidade Federal da Integração Latino-Americana, Instituto Latino-Americano de Ciências da Vida e da Natureza, Programa de Pós-Graduação em Física Aplicada. Foz do Iguaçu - PR, 2026.
Orientador: Eduardo do Carmo.

1. Cristais Líquidos. 2. Estatística - Modelo de Maier-Saupe. 3. Física - Teoria de Landau-de Gennes. I. Carmo, Eduardo do. II. Título.

CDU 538.9

Krzyzanowski, Gabriel

Thermotropic Liquid Crystal Models with Multicritical Points/Gabriel Krzyzanowski. – Foz do Iguaçu: ILACVN/UNILA, 2026.

XI, 52 p.: il.; 29, 7cm.

Orientador: Dr. Eduardo do Carmo

Dissertação (mestrado) – ILACVN/UNILA/Programa de Pós Graduação em Física Aplicada, 2026.

Referências Bibliográficas: p. 49 – 52.

1. Cristais Líquidos. 2. Modelo de Maier–Saupe. 3. Teoria de Landau-de Gennes. I. do Carmo, Dr. Eduardo. II. Universidade Federal da Integração Latino Americana, ILACVN, Programa de Programa de Pós Graduação em Física Aplicada. III. Título.

Dedico este trabalho ao meu pai, Pedro Barbosa de Oliveira, que me ensinou a ter calma e paciência ao encarar a vida. O senhor estará vivo eternamente nas memórias daqueles que lhe conheceram em vida.

AGRADECIMENTOS

"Happiness is only real when shared."
Christopher McCandless

Foram muitas as lições que aprendi durante esses dois anos de estudos. A mais importante, porém, é de que as alegrias da vida existem para serem compartilhadas. Com muito carinho, agradeço a todos que estiveram comigo nesse período, compartilhando as alegrias, dores e dificuldades.

Em especial, agradeço ao meu mestre *Eduardo do Carmo* cuja figura sempre me inspirou a ser um pesquisador e uma pessoa melhor. Agradeço por todas as reuniões e todo o apoio no desenvolvimento deste trabalho. Agradeço também por todo o suporte emocional em momentos difíceis que passei durante esse período. Levarei para toda vida as lições e ensinamentos que o senhor me passou com tanta alegria e entusiasmo.

Agradeço também a toda minha família. Considero um privilégio incalculável ter um lugar para chamar de casa. Agradeço particularmente a minha mãe, Janete Krzyzanowski, e a minha irmã, Nykolli Krzyzanowski. Passamos por momentos muito difíceis juntos, mas foram esses que nos uniram mais ainda e nos deram força para encarar as adversidades futuras.

Não poderia deixar de mencionar todos meus colegas, professores e servidores do programa de pós graduação em física aplicada da UNILA. Em especial, meus amigos do PTI, que estiveram presentes na minha rotina—Camila, Jhon, Judith, Jazmin, Eduardo, Dayra, Manoela e tantos outros. Foram vocês que fizeram meus dias mais leves.

Separo um parágrafo para agradecer a pessoa mais especial em minha vida durante essa jornada: *Luanna Aquino*. Palavras não são suficientes para descrever nossa amizade.

Por último, e mais importante, agradeço aos dois irmãos que a vida me deu: *Marhlon Bhrendon* e *Hussein Moussa*. Se a felicidade só é real quando compartilhada, foi com vocês meus irmãos que eu a compartilhei nesse período.

Resumo da Dissertação apresentada à PPGFISA/UNILA como parte dos requisitos necessários para a obtenção do grau de Mestre em Ciências (M.Sc.)

MODELOS PARA CRISTAIS LÍQUIDOS TERMOTRÓPICOS COM PONTOS MULTICRÍTICOS

Gabriel Krzyzanowski

Março/2026

Orientador: Dr. Eduardo do Carmo

Programa: Programa de Pós Graduação em Física Aplicada

O presente trabalho considera versões estendidas para a formulação de campo médio do modelo de rede de Maier-Saupe para cristais líquidos termotrópicos nemáticos. Primeiro, uma versão com a inclusão de variáveis de ocupação é apresentada e, em seguida, estuda-se uma versão com o acréscimo de graus de liberdade que mimetiza uma interação polar, tendo em vista a recente confirmação da existência uma fase ferronemática para certos materiais formados por moléculas com forte polarização. Os modelos são analisados por meio de técnicas modernas em física estatística e ferramentas numéricas, bem como através de um contato com a teoria fenomenológica de Landau–de Gennes. Os diagramas de fase resultantes e as características das transições de fase são examinados em termos da topologia das fases e do comportamento crítico, evidenciando concordância qualitativa com observações experimentais disponíveis.

Abstract of Dissertation presented to PPGFISA/UNILA as a partial fulfillment of the requirements for the degree of Master of Science (M.Sc.)

THERMOTROPIC LIQUID CRYSTAL MODELS WITH MULTICRITICAL POINTS

Gabriel Krzyzanowski

March/2026

Advisor: Dr. Eduardo do Carmo

Department: Postgraduate Program in Applied Physics

The present work considers extended versions of the mean-field formulation of the Maier–Saupe lattice model for thermotropic nematic liquid crystals. First, a version including occupation variables is introduced. Subsequently, a second version is investigated in which additional degrees of freedom are incorporated to mimic a polar interaction, motivated by the recent experimental confirmation of a ferronematic phase in certain materials composed of strongly polar molecules. The models are analyzed using modern techniques of statistical physics and numerical methods, as well as through connections with the phenomenological Landau-de Gennes theory. The resulting phase diagrams and the nature of the phase transitions are examined in terms of phase topology and critical behavior, showing qualitative agreement with available experimental observations.

CONTENTS

LIST OF FIGURES

INTRODUCTION

"Daqui inferi eu que a vida é o mais engenhoso dos fenômenos, porque só aguça a fome, com o fim de deparar a ocasião de comer, e não inventou os calos, senão porque eles aperfeiçoam a felicidade terrestre. Em verdade vos digo que toda a sabedoria humana não vale um par de botas curtas."
Machado de Assis

The notion that materials can exist in different *phases* is well known both in academia and in everyday experience. It is common knowledge that water crystallizes into a solid below a certain temperature and vaporizes above another. A powerful argument is revealed when one first examines this peculiar behavior: the arrangement of the molecules composing a material determines its behavior. When molecules are arranged in a regular and periodic structure, the material forms a crystal; when positional order is lost, a liquid phase emerges; and when the molecules are free from any restriction a gaseous phase takes place. This reasoning may suggest that matter exists only in three states—solid, liquid and gas. However, such a classification is far from complete.

In particular, certain materials—known as *mesomorphic phases*—exhibit intermediate behavior between that of crystalline solids and liquid phases, for that reason they are commonly referred to as *liquid crystals* (DE GENNES and PROST (1993)). To understand the nature of these materials, the concept introduced in the previous paragraph must be extended. A material is said to be in a crystalline phase when its constituent molecules display two types of long-range order: positional order of their centers of mass and orientational order of their molecular axes (GRAMSBERGEN *et al.* (1986)). Upon melting into a liquid, both kinds of ordering disappear at the same temperature. However, in mesomorphic phases the positional order is destroyed while orientational order persists over long distances. In this regime, the material retains fluidity while maintaining a degree of molecular alignment, thereby defining the *liquid-crystalline state*.

Depending on the molecular arrangement and the associated symmetry of the phase, liquid crystals are commonly classified into *nematic*, *cholesterics*, *smectics*, and *columnar* phases (Fig. 1). According to ANDRIENKO (2018), from a chemical perspective, molecules forming nematic phases have anisotropic shape, often with rigid molecular backbones which define the long axes of molecules. With the

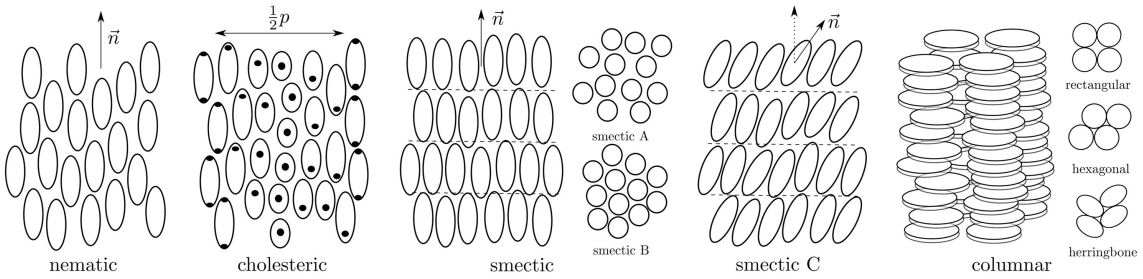

Figure 1: *Molecular arrangement in liquid crystalline phases. The vector $\vec{n}$ represents the preferred direction of alignment. (ANDRIENKO (2018)).*

exception of the columnar phase—whose constituent molecules are usually stacked flat-shaped discotic molecules—the remaining phases differ from the nematic only in terms of symmetry.

In the nematic phase, there is no long-range positional order of the molecular centers of mass; however, the molecular orientations tend to align along a preferred direction, known as the director $\vec{n}$. In the cholesterics phase, the director varies throughout the medium in a regular way, giving rise to a helical superstructure characterized by a pitch, defined as the distance p along the helical axis over which the director rotates by 2π. In smectic phases, molecules are arranged into well-defined layers, exhibiting partial correlation in their positions. In the smectic A phase, the molecular long axis are on average perpendicular to the layers, whereas in smectic B and additional two-dimensional hexagonal order develops within each layer. In smectic C, the director is tilted with respect to the layer normal vector. Finally, in a columnar phase, molecules assemble into cylindrical columns that form two dimensional lattices.

Once the general aspects of the liquid-crystalline phase was presented, it is worth outlining the magnitude of the key technological implications arising from liquid crystal science. Applications of liquid-crystal technology have evolved into a multi-trillion-dollar industry. Their technological relevance stems primarily from electrically controllable birefringence. Two key mechanisms underlie this functionality. In standard display technologies, the dominant mechanism is dielectric torque, which operates in materials with positive dielectric anisotropy and does not require the presence of ionic species (BLINOV (2010)). In contrast, the Carr–Helfrich effect occurs in nematic systems with negative dielectric anisotropy and appreciable ionic conductivity (HELFRICH (1969)). In this regime, the application of an external electric field leads to the redistribution of mobile ionic impurities, generating space charges that induce reorientation and flow of the liquid-crystal molecules (CHEN (2011)). This reorientation enables precise control over the molecular alignment and, consequently, over the optical axis of the medium.

Controlling the polarization state of linearly polarized incident light is the key for

the most pervasive application of liquid crystal in industry: the **LCD** (*Liquid Crystal Display*). Nowadays, the technology is, in principle, still based on the original work from half a century ago with some improvements in materials (KIM and SONG (2009)). While displays offering excellent viewing angles and video performance have been well established, fundamental display research has increasingly focused on emerging technologies, including 3D visions, holographic displays and AV-VR (*Artificial Vision–Virtual Reality*) devices (DIERKING (2025)).

With regard to fundamental research, interest has shifted toward a broader range of questions, closely related to other disciplines, including fundamental physics, optics and photonic, topology, biology, and nanotechnology. This increasing overlap of topics reflects a growing synergy and multi-disciplinarity within the field (DIERKING (2025)). Nevertheless, research on structure-property relationships remains an active and compelling area of investigation. Of particular relevance to the present work are the recent developments surrounding what has been called the "holy grail" of liquid-crystal materials: the **ferroelectric nematic phase** (CRUICKSHANK (2024)). On the theoretical side, concepts from mathematical physics have found increasing applications in liquid-crystal research, for example, the recent studies on topology (TUBIANA *et al.* (2024)). Finally, one must also mention that the role of computer modeling and simulation has become ever more prominent, now constituting and essential component of research in this area (WILSON *et al.* (2022)).

In the present work, what follows is a research in fundamental physics: phase transitions and symmetry-breaking phenomena are studied through simple models for thermotropic nematic liquid-crystal within the mean-field framework. Two extensions of the classical Maier–Saupe model are considered: a site-diluted version, motivated by theoretical and experimental results (LENART *et al.* (2012); SIMÕES *et al.* (2013)), designed to probe the known critical-like behavior of the nematic-isotropic transition; and a ferroelectric coupled version, formulated within the theoretical framework proposed by ETXEBARRIA *et al.* (2022), aimed at describing recent developments on experimental research within this field.

In the context of the canonical ensemble—and grand-canonical ensemble for the site-diluted model—the corresponding free-energy functional is derived and analyzed through numerical minimization, allowing the construction of phase diagrams and the characterization of phase behavior. Additionally, the Landau–de Gennes phenomenological theory is employed to gain deeper insights into the critical properties, the nature of the phase transition, and the role of symmetry in the phases discussed. Multicriticality is then investigated. A multicritical point is a point in parameter space where two or more lines of phase transitions meet, typically separating regions with distinct types of ordering or different transition character. Qualitatively, it marks a change in the fundamental mechanism by which the system undergoes a

phase transition, such as from first-order to continuous behavior.

The work is organized as follows. The first chapter introduces the concept of an order parameter suitable for characterizing macroscopic order and symmetry in liquid-crystal materials. The second chapter is focused on reviewing well-established theoretical models in statistical physics, with the Ising model presented as a pedagogical example to illustrate the analytical and numerical techniques employed in the subsequent chapters. The third chapter focus on a site-diluted extension of the Maier–Saupe model, in which a modification of the classical framework is used to investigate the critical-like behavior of the nematic-isotropic phase transition. Finally, the fourth chapter introduces a kind of polar Maier–Saupe model aimed at stabilizing a ferronematic phase and analyzing the nature of the associated phase transition.

CHAPTER 1

THE NEMATIC ORDER PARAMETER

"Le vent se lève!... il faut tenter de vivre!"
Paul Valéry

Nematic liquid crystal materials exhibit long-range orientational order. At the microscopic level, this implies that the molecular orientational vectors $\tilde{\mathbf{n}}_i$ are distributed within a cone of aperture angle θ centered around a vector $\tilde{\mathbf{N}}$, named director (Figure 1.1). A phase transition to an isotropic phase—when there is no preferred direction of alignment—is characterized by introducing an *order parameter*.

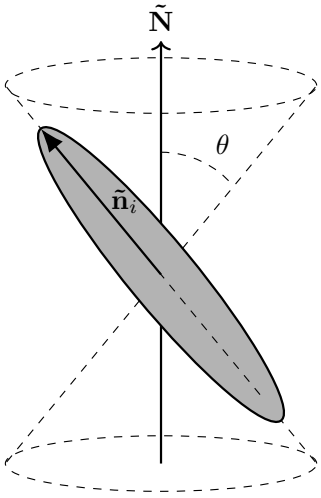

Figure 1.1: *Molecular order in a nematic liquid crystal.* $\tilde{\mathbf{N}}$ *is the director.*

The basic mathematical requirements for an order parameter Q are:

1. $Q = 0$ in the less ordered (isotropic) phase;

2. $Q \neq 0$ if exists any orientational ordering.

In a ferromagnetic material, macroscopic order is described by the magnetization vector, whose alignment with a preferred direction can be quantified by the

cosine of the angle between them. By analogy, in a nematic liquid crystal system, a macroscopic order parameter may be defined by looking at the angle θ between the preferred direction of alignment, which is called the director $\tilde{\mathbf{N}}$, and a molecule's local symmetry axis $\tilde{\mathbf{n}}_i$. Consequently, defining the order parameter as

$$\langle \cos\theta \rangle = \frac{1}{N} \sum_i \cos\theta_i, \tag{1.1}$$

yields a value of 1 in a system with N molecules when all $\tilde{\mathbf{n}}_i$ molecular vectors are aligned in one preferred direction, and a value of 0 in the isotropic phase. The problem with this approach is that it does not account for the head-to-tail symmetry of rod-like molecules where the directions $\tilde{\mathbf{n}}_i$ and $-\tilde{\mathbf{n}}_i$ are equivalent. For a perfectly ordered nematic head-to-tail symmetry implies that half the molecules have $\theta_i = 0$ and the other half $\theta_i = \pi$. In this case, equation 1.1 yields a value of 0. Hence, in a nematic liquid crystal, a different approach is required to define a parameter quantifying its macroscopic order.

Therefore, the central objective of this chapter is to define an order parameter capable of capturing macroscopic order, as well as to elucidate its role in symmetry breaking and in the characterization of different types of phase transitions. In addition, this chapter provides the conceptual and mathematical framework necessary for the theoretical models developed in the subsequent chapters.

1.1 Microscopic Approach

The analysis begins with the simplest type of molecular model, in which the molecules are described as rigid, axially symmetric rods possessing cylindrical symmetry around $\tilde{\mathbf{n}}$. When the nematic axis $\tilde{\mathbf{N}}$ is chosen as the z-axis of the (x, y, z) laboratory frame, the vector $\tilde{\mathbf{n}}$ is fully specified by the polar angles θ and ϕ:

$$n_x = \sin\theta \, \cos\phi,$$
$$n_y = \sin\theta \, \sin\phi,$$

and

$$n_z = \cos\theta.$$

Following DE GENNES and PROST (1993); MAIER and SAUPE (1958a, 1959, 1960), the state of alignment of the rods is described by a distribution function $f(\theta, \phi)\, d\Omega$, which gives the probability of finding a rod within a small solid angle $d\Omega = \sin\theta \, d\theta \, d\phi$ about the direction (θ, ϕ). The lowest term in a multipole expansion capable of capturing information about the phase order—despite the rotational

symmetry about $\tilde{\mathbf{n}}$, which removes the ϕ dependence on f—is defined by the thermal average

$$S = \frac{1}{2}\langle(3\cos^2\theta - 1)\rangle = \int f(\theta)\frac{1}{2}(3\cos^2\theta - 1)d\Omega, \tag{1.2}$$

which follows the normalization condition

$$\int_0^{2\pi} d\phi \int_0^{\pi} f(\theta)\sin\theta\, d\theta = 1 \tag{1.3}$$

In particular, if $f(\theta)$ is peaked around $\theta = 0$ and $\theta = \pi$, then $S = 1$. On the other hand, if $f(\theta)$ is completely independent of θ, corresponding to random molecular orientations, then $S = 0$.

The second order Legendre polynomial in equation 1.2 represents the lowest-order rotational invariant compatible with the head-to-tail symmetry of rod-like molecules in nematic phases.

1.2 Tensorial Description

The generalization of the order parameter for different molecules and arbitrary frame of references follows naturally from equation 1.2 by considering that $\cos^2\theta = (\tilde{\mathbf{N}}\cdot\tilde{\mathbf{n}})^2$, which leads to

$$\mathcal{Q}^{\mu\nu} = \frac{1}{2}\langle 3n^\mu n^\nu - \delta_{\mu\nu}\rangle, \tag{1.4}$$

where $\mu, \nu = x, y, z$ are indices referring to the laboratory frame. The tensor $\mathcal{Q}^{\mu\nu}$ is symmetric and traceless by construction, and remains invariant under the transformation $\tilde{\mathbf{n}} \to -\tilde{\mathbf{n}}$, reflecting the apolar nature of nematic order.

For a nematic phase aligned along the z-axis, the *scalar order parameter* is defined as

$$S \equiv \mathcal{Q}^{zz} = \left\langle \frac{3}{2}\cos^2(\theta) - \frac{1}{2}\right\rangle. \tag{1.5}$$

From this definition, it follows that

$$\mathcal{Q}^{xx} = \left\langle \frac{3}{2}\sin^2(\theta)\cos^2(\phi) - \frac{1}{2}\right\rangle = \left\langle \frac{3}{4}\sin^2(\theta) - \frac{1}{2}\right\rangle = -\frac{S}{2},$$

$$\mathcal{Q}^{yy} = \left\langle \frac{3}{2}\sin^2(\theta)\sin^2(\phi) - \frac{1}{2}\right\rangle = \left\langle \frac{3}{4}\sin^2(\theta) - \frac{1}{2}\right\rangle = -\frac{S}{2},$$

and the off-diagonal components vanish. Hence, partial nematic order along the z-axis is represented by the tensor

$$\mathcal{Q} = \begin{pmatrix} -\frac{S}{2} & 0 & 0 \\ 0 & -\frac{S}{2} & 0 \\ 0 & 0 & S \end{pmatrix}. \tag{1.6}$$

For a nematic phase oriented along an arbitrary direction $\tilde{\mathbf{N}}$, the components of the order tensor take the uniaxial form

$$\mathcal{Q}^{\mu\nu} = S\Big(\frac{3}{2}n^{\mu}n^{\nu} - \frac{1}{2}\delta_{\mu\nu}\Big). \tag{1.7}$$

This tensorial order parameter provides the foundation for the subsequent sections for the symmetry-based and mean-field theories discussed in subsequent chapters.

1.3 Beyond uniaxial order

In order to go beyond usual uniaxial order, a geometrical approach is considered to build the tensorial order parameter.

Consider an ellipsoid $\hat{E}$ defined along three mutually orthonormal directions $\hat{p}$, $\hat{q}$, and $\hat{r}$ (SIMOES and DA SILVA (2011)). The surface of the ellipsoid is described by the quadratic form

$$\hat{E}_{ij}x_i x_j = 1, \tag{1.8}$$

where **the Einstein's sum rule over repeated indices is adopted**, and

$$\hat{E}_{ij} = \frac{\hat{p}_i\hat{p}_j}{r_1^2} + \frac{\hat{q}_i\hat{q}_j}{r_2^2} + \frac{\hat{r}_i\hat{r}_j}{r_3^2}, \qquad i,j = \{1,2,3\}. \tag{1.9}$$

An arbitrary vector $\vec{x}$ may be decomposed along the orthonormal basis $\{\hat{p},\hat{q},\hat{r}\}$ as

$$x_i = p_i(p_j x_j) + q_i(q_j x_j) + r_i(r_j x_j) = (\hat{p}_i\hat{p}_j + \hat{q}_i\hat{q}_j + \hat{r}_i\hat{r}_j)x_j, \tag{1.10}$$

which implies the completeness relation

$$\hat{p}_i\hat{p}_j + \hat{q}_i\hat{q}_j + \hat{r}_i\hat{r}_j = \delta_{ij}. \tag{1.11}$$

It is convenient to introduce the traceless second-rank tensors

$$\hat{\mathbf{P}}_{ij} = \frac{3}{2}\hat{p}_i\hat{p}_j - \frac{1}{2}\delta_{ij}, \qquad \hat{\mathbf{Q}}_{ij} = \frac{3}{2}\hat{q}_i\hat{q}_j - \frac{1}{2}\delta_{ij}, \text{ and} \qquad \hat{\mathbf{R}}_{ij} = \frac{3}{2}\hat{r}_i\hat{r}_j - \frac{1}{2}\delta_{ij}. \tag{1.12}$$

In terms of these tensors, the ellipsoid matrix may be rewritten as

$$\hat{E}_{ij} = \frac{2}{3}\left(\frac{\hat{\mathbf{P}}_{ij}}{r_1^2} + \frac{\hat{\mathbf{Q}}_{ij}}{r_2^2} + \frac{\hat{\mathbf{R}}_{ij}}{r_3^2}\right) + \frac{1}{3}\left(\frac{1}{r_1^2} + \frac{1}{r_2^2} + \frac{1}{r_3^2}\right)\delta_{ij}. \tag{1.13}$$

This expression naturally separates into an isotropic contribution and a traceless

anisotropic deformation tensor,

$$\hat{E}_{ij} = \Delta E_{ij} + \frac{1}{r_S^2}\delta_{ij} \text{ and } \qquad \frac{1}{r_S^2} = \frac{1}{3}\left(\frac{1}{r_1^2} + \frac{1}{r_2^2} + \frac{1}{r_3^2}\right). \tag{1.14}$$

The tensor ΔE_{ij} quantifies the anisotropy of the molecular shape.

Three distinct cases may be identified:

- **Isotropic molecule**: $r_1 = r_2 = r_3 = r$, for which

$$\Delta E_{ij}^I = \frac{2}{3r^2}(\hat{\mathbf{P}}_{ij} + \hat{\mathbf{Q}}_{ij} + \hat{\mathbf{R}}_{ij}) = 0. \tag{1.15}$$

- **Uniaxial molecule**: $r_1 = r_2 \neq r_3$, leading to

$$\Delta E_{ij}^U = \frac{2}{3}\left(\frac{1}{r_3^2} - \frac{1}{r_1^2}\right)\hat{\mathbf{R}}_{ij}. \tag{1.16}$$

- **Biaxial molecule**: $r_1 \neq r_2 \neq r_3$, for which

$$\Delta E_{ij}^B = \frac{2}{3}\left(\frac{1}{r_1^2} - \frac{1}{r_3^2}\right)\hat{\mathbf{P}}_{ij} + \frac{2}{3}\left(\frac{1}{r_2^2} - \frac{1}{r_3^2}\right)\hat{\mathbf{Q}}_{ij}. \tag{1.17}$$

For the biaxial case, it is useful to define the eccentricity parameters

$$e_1 = \frac{2}{3}\left(\frac{1}{r_1^2} - \frac{1}{r_3^2}\right) \text{ and } \qquad e_2 = \frac{2}{3}\left(\frac{1}{r_2^2} - \frac{1}{r_3^2}\right), \tag{1.18}$$

such that

$$\Delta E_{ij}^B = e_1\hat{\mathbf{P}}_{ij} + e_2\hat{\mathbf{Q}}_{ij}. \tag{1.19}$$

Using the identity $\hat{\mathbf{P}}_{ij} + \hat{\mathbf{Q}}_{ij} + \hat{\mathbf{R}}_{ij} = 0$, the biaxial deformation tensor may be recast as

$$\begin{aligned}\Delta E_{ij}^B &= \frac{e_1 + e_2}{2}(\hat{\mathbf{P}}_{ij} + \hat{\mathbf{Q}}_{ij}) + \frac{e_1 - e_2}{2}(\hat{\mathbf{P}}_{ij} - \hat{\mathbf{Q}}_{ij}) \\ &= -\frac{e_1 + e_2}{2}\hat{\mathbf{R}}_{ij} + \frac{e_1 - e_2}{2}(\hat{\mathbf{P}}_{ij} - \hat{\mathbf{Q}}_{ij}).\end{aligned} \tag{1.20}$$

Defining

$$S = -\frac{e_1 + e_2}{2} = \frac{1}{r_3^2} - \frac{1}{r_S^2} \text{ and } \qquad \eta = \frac{e_1 - e_2}{2} = \frac{1}{3}\left(\frac{1}{r_1^2} - \frac{1}{r_2^2}\right), \tag{1.21}$$

the biaxial deformation tensor finally assumes the form

$$\Delta E_{ij}^B = S\,\hat{\mathbf{R}}_{ij} + \eta(\hat{\mathbf{P}}_{ij} - \hat{\mathbf{Q}}_{ij}). \tag{1.22}$$

The parameter S defined in equation 1.21 is physically equivalent to the scalar order parameter of equation 1.5. The thermal average over the equation 1.22 provides a compact representation of the macroscopic orientational order in systems composed of molecules that can exhibit biaxial order (SIMOES and DA SILVA (2011)).

1.4 Symmetry of liquid-crystalline phases

The primary distinction between the *nematic* and *isotropic* phase lies in their degree of symmetry and molecular ordering. An isotropic liquid is a state where the molecules possess no long-range order in both the positions of molecular centers of mass and their direction of alignment. In this phase, the correlation function is isotropic—meaning it depends only on the distance between molecules. As a consequence, macroscopic response functions—such as the magnetic susceptibility—are uniform in all spatial directions DE GENNES and PROST (1993).

In contrast, the nematic phase is defined by the breaking of rotational symmetry through the emergence of long-range orientational order, while long-range positional order remains absent, as illustrated in Figure 1.2. In this phase, molecules tend to align their principal axes along a common direction specified by a unit vector known as the director $\tilde{\mathbf{N}}$. This partial alignment introduces anisotropy into the physical properties of the material. As a result, the nematic phase possesses lower symmetry than the isotropic phase (GRAMSBERGEN *et al.* (1986)). The isotropic–nematic transition therefore constitutes an example of spontaneous rotational symmetry breaking.

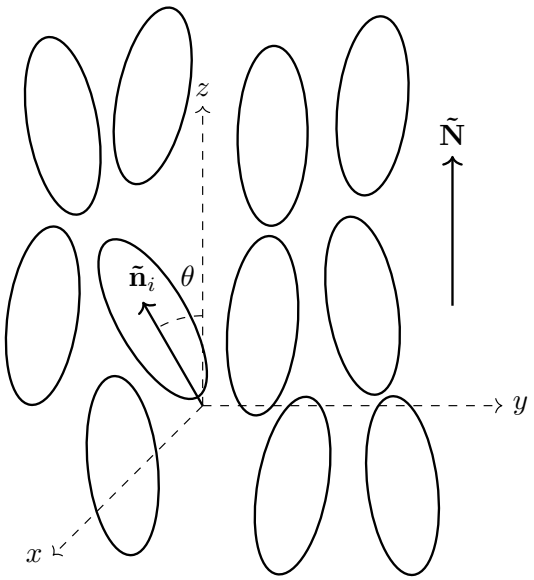

Figure 1.2: *Nematic Ordering*

An important feature of nematic phases is their *apolar nature*. As stated before, molecular directions $\tilde{\mathbf{n}}_i$ and $-\tilde{\mathbf{n}}_i$ are indistinguishable in a nematic phase meaning that, on average, an equal number of molecules point "up" or "down", resulting in zero macroscopic net polarization. The nematic phase therefore behaves optically as a uniaxial medium with inversion symmetry. This property plays a crucial role in later discussions, particularly in Chapter 4, where phases with broken inversion symmetry—such as ferroelectric nematics—are examined.

Several complementary approaches can be employed to relate the symmetry of a phase to an appropriate choice of order parameter. Molecules with rigid, elongated shapes—such as those depicted in Figure 1.2—are particularly effective at stabilizing nematic mesophases. Upon melting, thermal fluctuations generally overcome intermolecular forces, destroying both positional and orientational order. However, for rod-like molecules, there exists an intermediate temperature range in which thermal energy is sufficient to disrupt positional order while leaving orientational order intact, leading to the formation of a nematic phase.

From an experimental perspective, the presence of long-range orientational order prevents molecular anisotropy from averaging to zero. As a result, macroscopic quantities such as the dielectric permittivity become anisotropic and can be exploited as probes of phase symmetry (GRAMSBERGEN *et al.* (1986)). Alternatively, a more formal description may be constructed using group-theory arguments, in which the order parameter is defined solely on the basis of symmetry considerations, as originally proposed by LANDAU *et al.* (1980).

1.5 Free-energy and Phase Transition

From elementary considerations in statistical mechanics, the canonical partition function is defined as

$$\mathcal{Z}(T, \mathcal{H}) = \mathrm{Tr} \exp(-\beta \mathcal{H}), \tag{1.23}$$

where the trace is taken over all possible microscopic configurations specified by the Hamiltonian $\mathcal{H}$, and $\beta = 1/k_B T$ with k_B denoting Boltzmann's constant and T the absolute temperature. The canonical partition function is a measure of the volume occupied by the system in the phase space in the *canonical ensemble*.

The connection with thermodynamics is done by the Helmholtz free energy, which is related to the partition function by

$$\mathcal{F}(T, \mathcal{H}) = -k_B T \, \ln \mathcal{Z}(T, \mathcal{H}). \tag{1.24}$$

Macroscopic thermodynamic properties are, in general, obtained by differentiating the Helmholtz free energy with respect to the relevant thermodynamic variables

at fixed temperature. In this framework, the resulting relations define the thermodynamic equations of state, which connect macroscopic observables to external parameters.

In the context of mean-field theory, however, the free energy is expressed as a functional of appropriate order parameters that encode the degree of microscopic ordering. The equilibrium state of the system is then determined by minimizing this free-energy functional with respect to these order parameters (SALINAS (1997)). This minimization procedure leads to a set of self-consistent equations—referred to as mean-field equations of state—which determine the physical state of the system, such as the degree of molecular alignment. In many situations, particularly in the vicinity of a phase transition, the free-energy landscape may exhibit multiple local minima. The physically realized state is identified with the global minimum, as only this configuration corresponds to a thermodynamically stable phase. In the classical theory of phase transitions, the local minima are identified with metastable thermodynamic states (DE GENNES and PROST (1993)).

The classification of phase transitions is determined by the behavior of the free energy and its derivatives and the associated order parameters. A phase transition is signaled by a nonanalyticity in a thermodynamic potential, such as the free energy. If one or more first derivatives of the free energy are discontinuous and the order parameter exhibits a finite jump, the transition is classified as first order. By contrast, if the first derivatives remain continuous while second derivatives become discontinuous or diverge, the transition is referred to as continuous, higher order, or critical (YEOMANS (1992)). Such continuous transitions are typically accompanied by a divergent susceptibility, an infinite correlation length, and power-law decay of correlation functions. In general, the NI transition is first order and the divergence of the susceptibility, if it occurs, is located at the spinodal point rather than at the actual transition temperature.

1.6 Scope and connection to theoretical models

In this chapter, an appropriate local order parameter (DE GENNES and PROST (1993)) was introduced and derived. The symmetry properties of the nematic and isotropic phases were analyzed, and the fundamental theoretical elements that underpin the remainder of this thesis were established.

In the next chapter, the basic models will be examined within this framework. The microscopic Maier–Saupe model will be introduced and solved within the mean-field approximation, and a phenomenological macroscopic description based on Landau theory will be presented to address symmetry breaking and the emergence of multicritical points using the previously defined order parameter.

CHAPTER 2

THEORETICAL MODELS FOR LIQUID CRYSTALS

"And what can life be worth if the first rehearsal for life is life itself?"
Milan Kundera

The concept of "models" plays a central role in scientific investigation and admits multiple interpretations depending on the context. Following WALLACE (1996), a model may be understood as an analogue or analogy that assists or promotes the gradual understanding of something not readily grasped in sense experience. In this sense, models function as idealized and simplified descriptions capable of capturing the essential behavior of complex natural systems. Guided by the principle of progressing "from the more known to the less known", modeling serves as a powerful tool for uncovering the intelligible structures underlying causes of nature.

In statistical mechanics, models are introduced by idealizing physical attributes in order to render the underlying structure of many-body systems more intelligible. For example, the Einstein model of a crystal simplifies the complex vibrational modes of a solid into a collection of independent harmonic oscillators (SALINAS (1997)). Such models are said to be *exactly solvable*, in the sense that their energy spectra can be determined analytically, allowing for an explicit calculation of the partition function and thermodynamic quantities. However, the majority of physically relevant systems are not exactly solvable, as only a limited class of interacting many-body models admits closed-form solutions (CALLEN (1993)). In these cases, approximate methods such as variational principles, mean-field theories, and numerical simulations become essential tools for extracting physical insight.

In this context, the purpose of the present chapter is to introduce and analyze the fundamental theoretical models employed in the study of liquid crystalline systems. To establish the necessary conceptual and methodological background, the Ising model of interacting magnetic moments is first discussed as a pedagogical example. The Maier–Saupe model is then presented as a fundament of the microscopic description of thermotropic nematics, together with its solution within the mean-field approximation and its connection to phenomenological theories of phase transitions.

2.1 The Ising model as a pedagogical example

A remarkable example of an interacting many-body system is the spin-1/2 Ising model, first introduced by Lenz and Ising in 1925 (NISS (2005)). In this model, a classical spin random variable σ_i, which can take the values ± 1, is placed at each lattice site $i = 1, \ldots, N$. The system is described by the Hamiltonian

$$\mathcal{H} = -J \sum_{\langle ij \rangle} \sigma_i \sigma_j - H \sum_i \sigma_i, \tag{2.1}$$

where J is the exchange interaction—positive values favor parallel alignment and negative values favor antiparallel alignment of neighboring spins—$\langle ij \rangle$ denotes a sum over nearest-neighbor pairs, and H is an external magnetic field.

The first term in equation 2.1 is responsible for the cooperative behavior of the system and for the emergence of a phase transition. While the one-dimensional case can be solved exactly and exhibits a phase transition only at zero temperature, obtaining exact solutions in higher dimensions is considerably more difficult. The exact solution of the two-dimensional Ising model in the absence of a magnetic field was first obtained by Onsager in 1944, whereas the three-dimensional model remains unsolved.

The spin variables σ_i admit multiple physical interpretations. They may represent magnetic moments pointing up or down at each lattice site; alternatively, σ_i can label the occupation of a site by atoms of type A or B, as in binary alloys, or even serve as an occupation variable indicating the presence or absence of a particle at a given site. The latter interpretation will be particularly relevant in the next chapter. These different realizations highlight the universal character of the Ising model and its broad applicability across distinct physical systems.

Solving the model amounts to solve the canonical partition function

$$\mathcal{Z}_N = \mathcal{Z}(T, H, N) = \sum_{\{\sigma_i\}} \exp\left(-\beta \mathcal{H}\right), \tag{2.2}$$

where the sum is taken over all possible configurations of the spin variables. From the partition function, the magnetic free energy per lattice site is obtained as

$$g = g(T, H) = \lim_{N \to \infty} \left[-\frac{1}{\beta N} \ln \mathcal{Z} \right]. \tag{2.3}$$

As a first pedagogical step, the model is solved in one dimension using the transfer-matrix technique.

2.1.1 Ising Model in One Dimension

Following SALINAS (1997), in one dimension the Ising Hamiltonian takes the form

$$\mathcal{H} = -J \sum_i \sigma_i \sigma_{i+1} - H \sum_i \sigma_i. \tag{2.4}$$

The corresponding canonical partition function can be written as

$$\mathcal{Z}_N = \sum_{\{\sigma_i\}} \exp\left[K \sum_{i=1}^{N} \sigma_i \sigma_{i+1} + \frac{L}{2} \sum_{i=1}^{N} (\sigma_i + \sigma_{i+1}) \right], \tag{2.5}$$

with $K = \beta J$ and $L = \beta H$.

Imposing periodic boundary conditions, $\sigma_{N+1} = \sigma_1$, equation 2.5 may be rewritten as

$$\mathcal{Z}_N = \sum_{\sigma_1, \sigma_2, \ldots, \sigma_N} \prod_i T(\sigma_i, \sigma_{i+1}), \tag{2.6}$$

where

$$T(\sigma_i, \sigma_{i+1}) = \exp\left[K \sigma_i \sigma_{i+1} + \frac{L}{2} (\sigma_i + \sigma_{i+1}) \right]. \tag{2.7}$$

This expression naturally leads to the definition of the *transfer matrix*

$$\mathbf{T} = \begin{pmatrix} T(+1,+1) & T(+1,-1) \\ T(-1,+1) & T(-1,-1) \end{pmatrix} = \begin{pmatrix} \exp(K+L) & \exp(-K) \\ \exp(-K) & \exp(K-L) \end{pmatrix}. \tag{2.8}$$

Using the properties of the transfer matrix, the canonical partition function can be expressed as

$$\mathcal{Z}_N = \mathrm{Tr}(\mathbf{T})^N = \lambda_1^N + \lambda_2^N, \tag{2.9}$$

where $\lambda_{1,2}$ are the eigenvalues of $\mathbf{T}$, given by

$$\lambda_{1,2} = e^K \cosh L \pm \left[e^{2K} \cosh^2 L - 2 \sinh(2K) \right]^{1/2}. \tag{2.10}$$

In the thermodynamic limit, $N \to \infty$, the largest eigenvalue dominates, and the free energy per site is given by

$$g(T, H) = \lim_{N \to \infty} \left[-\frac{1}{\beta N} \ln \mathcal{Z} \right] = -\frac{1}{\beta} \ln \lambda_1. \tag{2.11}$$

This exact expression fully determines the thermodynamic properties of the one-dimensional Ising model. Based on general arguments originally proposed by Landau, it follows that this system cannot sustain a phase with long-range order at finite temperature. Consequently, the critical point of the one-dimensional Ising model is located at zero temperature.

2.1.2 Monte Carlo Method

Exact analytical solutions of the Ising model in dimensions greater than two remain unavailable. As a result, much of the understanding of its critical behavior has been obtained through experimental observations and through numerical simulations, which constitute the focus of this subsection. Among the most widely used numerical techniques in statistical mechanics is the *Monte Carlo method*. Monte Carlo methods comprise a class of computational algorithms based on stochastic sampling to evaluate thermodynamic quantities. In the present context, such methods are employed to estimate the mean magnetization as a function of temperature for the Ising model, with $H = 0$, by that means providing insight into the phase behavior of the system.

For each temperature within a selected range, a lattice of spins is initialized and allowed to reach thermal equilibrium using importance-sampling algorithms, such as the Metropolis algorithm (METROPOLIS *et al.* (1953)), which generate a Markov chain of spin configurations satisfying detailed balance and ergodicity. Once equilibration is achieved, the spins are repeatedly updated and the total magnetization is measured and recorded. From these data, the average squared magnetization and its associated statistical uncertainty are computed. To improve numerical efficiency and reduce statistical noise, the simulations can be performed multiple times independently—often in parallel—and the resulting averages combined. Representative results obtained using this procedure are shown in Figure 2.1. The convergence of the algorithm toward the analytical result improves as $L \to \infty$. However, the computational efficiency deteriorates significantly with increasing L, leading to substantially longer simulation times. This scaling behavior constitutes the main limitation of the method. Nevertheless, this method presents itself as a robust and versatile alternative in situations where analytical solutions are not available.

2.1.3 Curie-Weiss model

Many statistical models can not be solved analytically, then some approximation methods become necessary. Mean-field theory is a statistical framework in which each molecule or spin is assumed to interact with an average field generated by all other particles in the system, thereby neglecting specific local correlations and fluctuations (CALLEN (1993)). In the Ising model this approximation is implemented through the *Curie-Weiss* Hamiltonian,

$$\mathcal{H}_{\mathcal{CW}} = -\frac{J}{2N}\sum_{i=1}^{N}\sum_{j=1}^{N}\sigma_i\sigma_j - H\sum_{i=1}^{N}\sigma_i, \tag{2.12}$$

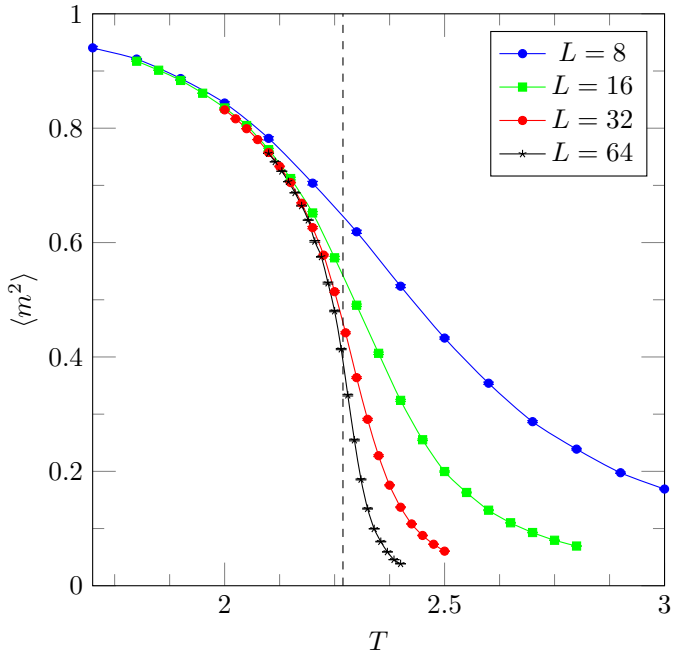

Figure 2.1: *Mean squared magnetization as a function of temperature for the two dimensional Ising model. The parameter L represents the length of the square lattice. The dashed line in $T_c \approx 2.269$ represents the exact critical temperature at which the transition occurs (LEE and YANG (1952)).*

where each spin interacts equally with all others in the system SALINAS (1997). The interactions are therefore of infinite range but sufficiently weak—scaling as $1/N$—to ensure a well-defined thermodynamic limit.

The canonical partition function associated with the Curie–Weiss model can be written as

$$\mathcal{Z} = \sum_{\{\sigma_i\}} \exp\left[\frac{\beta J}{2N}\left(\sum_{i=1}^{N}\sigma_i\right)^2 + \beta H \sum_{i=1}^{N}\sigma_i\right]. \tag{2.13}$$

From equation 2.13, following the procedure detailed in the next section, the free-energy density functional can be obtained as

$$g(T, H; m) = \frac{1}{2}Jm^2 - \frac{1}{\beta}\ln\left[2\cosh\left(\beta Jm + \beta H\right)\right], \tag{2.14}$$

where m denotes the magnetization per particle.

In the thermodynamic limit, minimizing the free energy with respect to m yields the Curie–Weiss equation of state,

$$m = \tanh\left(\beta Jm + \beta H\right). \tag{2.15}$$

Equation 2.15 encapsulates the mean-field description of the Ising model and illustrates how spontaneous magnetization emerges within this approximation.

2.2 The Maier–Saupe Model

The Maier–Saupe theory of liquid crystals represents a historical milestone in the theoretical description of thermotropic nematic phases. Despite its conceptual simplicity, the theory successfully captures the essential features of the nematic–isotropic (N–I) phase transition. As stated in MAIER and SAUPE (1958b, 1959, 1960), "a theory of nematic liquids must above all provide an explanation for the existence of this long-range order, as well as for the order of magnitude of the degree of order and its temperature dependence". There is little doubt that this objective was achieved within the Maier–Saupe framework. In the context of nematic liquid crystals, the Maier–Saupe model plays a role analogous to the Weiss molecular-field approximation in ferromagnetic systems (DE GENNES and PROST (1993)).

2.2.1 Mean-field formulation

The mean-field character of the Maier-Saupe theory is due to the neglect of correlations between neighboring molecules in the nematic liquid phase (DE GENNES and PROST (1993)). As a result, the orientation of a given molecule is determined by an effective mean field that is independent of the instantaneous orientations of its neighbors. This mean field originates from the collective orientational state of all molecules in the system and therefore reflects the macroscopic order of the phase.

The Hamiltonian that defines the Maier-Saupe model in the mean-field version is written as

$$\mathcal{H} = -\frac{J}{2N}\sum_{i,j}\sum_{\mu,\nu} S_i^{\mu\nu} S_j^{\mu\nu}, \tag{2.16}$$

where

$$S_i^{\mu\nu} = \frac{3}{2} n_i^{\mu} n_i^{\nu} - \frac{1}{2}\delta_{\mu\nu} \tag{2.17}$$

denotes the components of the second-rank order tensor, defined with respect to the laboratory frame of reference, and $(\mu, \nu) = x, y, z$, with $\delta_{\mu\nu}$ representing the Kronecker delta.

The partition function in the canonical ensemble is given by

$$\mathcal{Z} = \mathrm{Tr}\exp(-\beta\mathcal{H}) = \mathrm{Tr}\exp\left(\frac{\beta J}{2N}\sum_{i,j}\sum_{\mu,\nu} S_i^{\mu\nu} S_j^{\mu\nu}\right), \tag{2.18}$$

where the trace $\mathrm{Tr} \equiv \sum_{\{\vec{n}_i\}}$ runs over all possible molecular orientations, equivalently over all configurations of the tensor components $S_i^{\mu\nu}$. The argument of the exponential can be simplified by exploiting its symmetry. In particular,

$\sum_{i,j} S_i^{\mu\nu} S_j^{\mu\nu} = \sum_i S_i^{\mu\nu} \cdot \sum_j S_j^{\mu\nu} = (\sum_i S_i^{\mu\nu})^2$.

Furthermore, the summation over Cartesian indices (μ, ν) can be factorized as a product. Equation (2.18) can therefore be rewritten as

$$\mathcal{Z} = \mathrm{Tr} \prod_{\mu,\nu} \exp\left(\frac{\beta J}{2N}\left(\sum_i S_i^{\mu\nu}\right)^2\right). \tag{2.19}$$

To decouple the quadratic term appearing in the exponential of equation 2.19 a powerful technique known as the *Hubbard-Stratonovich* transformation is introduced. The key identity in the method is simply an observation of the result of a Gaussian integral. In the present case, it takes the form

$$e^{\frac{\beta J}{2N}(\sum_i S_i^{\mu\nu})^2} = \sqrt{\frac{N\beta J}{2\pi}} \int_{-\infty}^{+\infty} dQ_{\mu\nu} e^{-\frac{N\beta J}{2} Q_{\mu\nu}^2 + \beta J Q_{\mu\nu} \sum_i S_i^{\mu\nu}}. \tag{2.20}$$

The usefulness of this identity is that if we substitute the exponential in equation 2.20 into equation 2.19 the quadratic therm in $S_i^{\mu\nu}$—containing all the degrees of freedom that have to be summed over—only occurs linearly, not quadratically.

Manipulating the partition function, it takes the form

$$\begin{aligned}\mathcal{Z} &= \mathrm{Tr} \prod_{\mu,\nu} \sqrt{\frac{N\beta J}{2\pi}} \int_{-\infty}^{+\infty} dQ_{\mu\nu} e^{-\frac{N\beta J}{2} Q_{\mu\nu}^2 + \beta J Q_{\mu\nu} \sum_i S_i^{\mu\nu}} \\ &= \left[\prod_{\mu,\nu} \sqrt{\frac{N\beta J}{2\pi}} \int_{-\infty}^{+\infty} dQ_{\mu\nu} e^{-\frac{N\beta J}{2} Q_{\mu\nu}^2}\right] \sum_{\{\vec{n}_i\}} \exp\left[\sum_{\mu,\nu} \beta J Q_{\mu\nu} \sum_i \left(\frac{3}{2} n_i^\mu n_i^\nu - \frac{1}{2}\delta_{\mu\nu}\right)\right]\end{aligned} \tag{2.21}$$

Since the molecules are independent in the mean-field approximation, the configurational sum factorizes, yielding

$$\mathcal{Z} = \left[\prod_{\mu,\nu} \sqrt{\frac{N\beta J}{2\pi}} \int_{-\infty}^{+\infty} dQ_{\mu\nu} e^{-\frac{N\beta J}{2} Q_{\mu\nu}^2}\right] \left\{\underbrace{\sum_{\{\vec{n}\}} \exp\left[\sum_{\mu,\nu} \beta J Q_{\mu\nu} \left(\frac{3}{2} n^\mu n^\nu - \frac{1}{2}\delta_{\mu\nu}\right)\right]}_{\mathcal{T}}\right\}^N. \tag{2.22}$$

At this point, in order to facilitate the analytical calculations, an orientational restriction is imposed to the nematic molecules: the Zwanzig discretization ZWANZIG (1963). While in the original Maier–Saupe model the molecular symmetry axes are free to rotate continuously with respect to the laboratory reference frame, in the present case, this restriction limits the orientation vector to the directions $\vec{n} = (\pm 1, 0, 0)$, $(0, \pm 1, 0)$, and $(0, 0, \pm 1)$. This approximation significantly simpli-

fies the analytical treatment of the model while preserving its qualitative physical behavior. The Zwanzig model preserves the first-order character of the NI transition but shifts the transition temperature by a numerical factor (DE OLIVEIRA and NETO (1986)). Proceeding with this discretization, the single-particle contribution $\mathcal{T}$ can be written as

$$\mathcal{T} = 2\exp\left(-\frac{1}{2}\beta J\sum_{\mu} Q_{\mu\mu}\right)\sum_{\mu}\exp\left(\frac{3\beta J}{2}Q_{\mu\mu}\right), \tag{2.23}$$

which leads to

$$\begin{aligned}\mathcal{Z} &= \left[\prod_{\mu,\nu}\sqrt{\frac{N\beta J}{2\pi}}\int_{-\infty}^{+\infty} dQ_{\mu\nu}e^{-\frac{N\beta J}{2}Q_{\mu\nu}^2}\right]\left\{2e^{-\frac{1}{2}\beta J\sum_{\mu}Q_{\mu\mu}}\sum_{\mu}e^{\frac{3\beta J}{2}Q_{\mu\mu}}\right\}^N \\ &= \left[\prod_{\mu,\nu}\sqrt{\frac{N\beta J}{2\pi}}\int_{-\infty}^{+\infty} dQ_{\mu\nu}\right]\exp\left\{-\frac{N\beta J}{2}\sum_{\mu,\nu}Q_{\mu\nu}^2 + N\ln\left[2e^{-\frac{1}{2}\beta J\sum_{\mu}Q_{\mu\mu}}\sum_{\mu}e^{\frac{3\beta J}{2}Q_{\mu\mu}}\right]\right\}.\end{aligned} \tag{2.24}$$

Finally, the partition function can be cast in the compact form

$$\mathcal{Z} = \left[\prod_{\mu,\nu}\sqrt{\frac{N\beta J}{2\pi}}\int_{-\infty}^{+\infty} dQ_{\mu\nu}\right]e^{-N\beta J f(\beta J;\mathbf{Q})}, \tag{2.25}$$

where

$$f(\beta J;\mathbf{Q}) = \frac{1}{2}\sum_{\mu,\nu}Q_{\mu\nu}^2 + \frac{1}{2}\sum_{\mu}Q_{\mu\mu} - \frac{1}{\beta J}\ln\sum_{\mu}e^{\frac{3\beta J}{2}Q_{\mu\mu}} - \frac{1}{\beta J}\ln 2 \tag{2.26}$$

is the Helmholtz free energy functional from where all the physical information of the system can be derived.

The auxiliary tensorial field $\mathbf{Q}$ gives the mean-field ordering of the system. In the laboratory reference frame, the local order tensor $\mathbf{S}$ can be made diagonal, and then the components $Q_{\mu\mu}$ can be directly identified with the macroscopic order parameters,

$$Q_{\mu\mu} = \left\langle\frac{1}{N}\sum_{i=1}^{N}S_i^{\mu\mu}\right\rangle, \tag{2.27}$$

where $\langle\cdots\rangle$ denotes a thermal average.

The values of $Q_{\mu\mu}$ physically realized are the ones that minimizes the free energy functional $f(\beta J;\mathbf{Q})$. The condition $\partial f/\partial Q_{\mu\mu}$ leads to the following equations of state:

$$Q_{\mu\mu} = -\frac{1}{2} + \frac{3}{2}\frac{e^{\frac{3\beta J}{2}Q_{\mu\mu}}}{\sum_{\mu}e^{\frac{3\beta J}{2}Q_{\mu\mu}}}. \tag{2.28}$$

Equation 2.28 implies the traceless condition $\sum_\mu Q_{\mu\mu} = 0$. By choosing $Q_{xx} = Q_{yy} = -S/2$ and $Q_{zz} = S$, the phase behavior of the nematic state can be analyzed in terms of a single scalar order parameter. Figure 2.2 shows the temperature dependence of the order parameter S. The transition temperature is determined by comparing the free-energy values of the ordered (nematic) and disordered (isotropic) solutions.

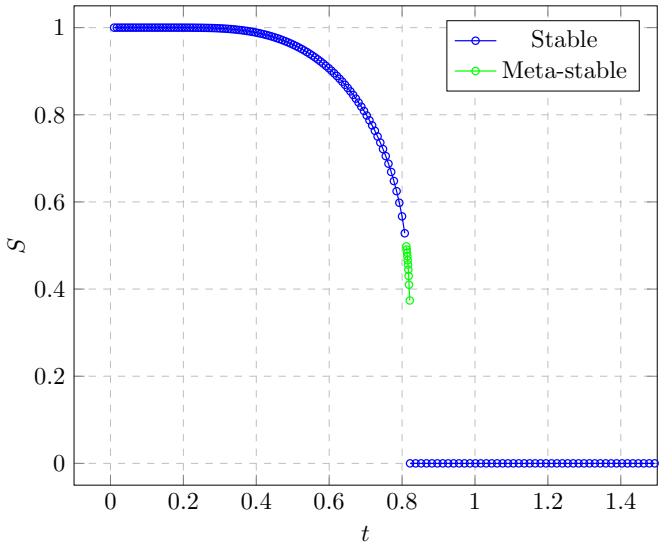

Figure 2.2: *Nematic order parameter as a function of temperature.*

The presence of a metastable region originates from the coexistence of competing minima in the free-energy landscape. As illustrated in Figure 2.3, near the transition temperature the free energy exhibits two local minima. In the vicinity of the transition, the nematic solution remains locally stable—signaled by a positive second derivative of the free energy—while its free-energy value exceeds that of the isotropic phase, indicating metastability.

2.3 Landau–de Gennes Theory of Phase Transition

Landau theory (LANDAU (1965)) may be viewed as a phenomenological expansion of the thermodynamic potential in the vicinity of a critical point. Its fundamental premise is that the nature of a phase transition can be understood primarily from symmetry considerations, rather than from the detailed microscopic interactions between molecules. Central to the theory is the concept of an order parameter—which explicitly encodes the change in symmetry associated with the transition. Implicit in this framework is the assumption that, near the transition temperature, the equilibrium properties of the system can be derived from a single functional of the order parameter, interpreted as a generalization of the free energy to nonequilibrium

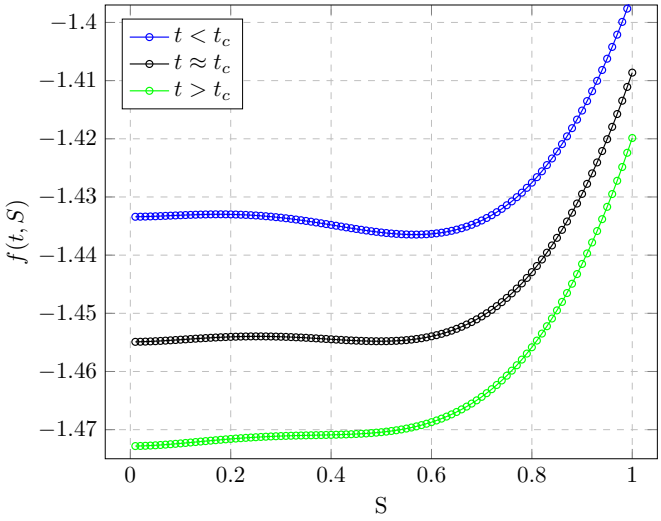

Figure 2.3: *Energy as a function of the order parameter around the critical temperature.*

configurations (GRAMSBERGEN *et al.* (1986)). Originally formulated to describe continuous (second-order) phase transitions, the theory was later extended by de Gennes to account for the first-order isotropic–nematic transition. This extension and its application constitute the focus of the present section.

Landau theory describes phase transitions through an expansion of the free energy in terms of an appropriate invariants of the order parameter Q. The generalization introduced in the Landau–de Gennes framework comes from the recognition that the isotropic–nematic transition is weakly first order and that, in the vicinity of the transition temperature, local orientational correlations persist even in the absence of macroscopic order. In other words, although the isotropic phase is globally disordered, molecules remain locally aligned within finite regions. This local order extends over a characteristic length scale known as the coherence length. Consequently, the effects associated with the phase transition are governed by fluctuations in the orientation of the optical axis (DE GENNES and PROST (1993)). Expanding the free energy in terms of the rotational invariants of the order parameter therefore provides a robust phenomenological description of the isotropic–nematic transition.

The simplest rotational invariants of a tensor are defined by

$$I_m \equiv \operatorname{Tr} \mathbf{Q}^m = \sum_{\mu} Q^m_{\mu\mu}, \tag{2.29}$$

where Tr is the trace operator and $m = 2, 3, 4, \ldots$. The free energy expansion close to a phase transition is thus written as

$$f = f_0 + \frac{a}{2} I_2 + \frac{b}{3} I_3 + \frac{c}{4} I_4 + \frac{d}{5} I_5 + \frac{e}{6} I_6 + \cdots \tag{2.30}$$

with f_0 equal to the free energy for the state with $\mathbf{Q} = 0$. Additionally, the coefficient of I_3 is not constrained to vanish by symmetry for nematics, because it is invariant under $\mathbf{Q} \to -\mathbf{Q}$.

Since the order parameter $\mathbf{Q}$ is a symmetric matrix, it can be shown that any invariant I_m with $m \geq 4$ can be expressed as a function of the lower-order invariants I_1, I_2, and I_3 (GRAMSBERGEN *et al.* (1986)). Furthermore, imposing the traceless condition $\operatorname{Tr}\mathbf{Q} = 0$ implies that $I_1 = 0$. As a consequence, the free energy in equation 2.26 can be written solely in terms of the invariants I_2 and I_3, using the relations

$$I_4 = \frac{1}{2}I_2^2, \quad I_5 = \frac{5}{6}I_2 I_3, \quad \text{and} \quad I_6 = \frac{1}{4}I_2^3 + \frac{1}{3}I_3^2. \tag{2.31}$$

To proceed, consider the expansion

$$\begin{aligned}\sum_\mu e^{\frac{3\beta J}{2}Q_{\mu\mu}} &= \sum_{m=0}^{\infty}\frac{1}{m!}\left(\frac{3\beta J}{2}\right)^m \sum_\mu Q_{\mu\mu}^m = \sum_{m=0}^{\infty}\frac{1}{m!}\left(\frac{3\beta J}{2}\right)^m I_m \\ &= 3 + \frac{1}{2!}\left(\frac{3\beta J}{2}\right)^2 I_2 + \frac{1}{3!}\left(\frac{3\beta J}{2}\right)^3 I_3 + \frac{1}{4!}\left(\frac{3\beta J}{2}\right)^4 I_4 + \frac{1}{5!}\left(\frac{3\beta J}{2}\right)^5 I_5 + \dots\end{aligned} \tag{2.32}$$

Retaining terms up to sixth order and using equation 2.31, one obtains

$$\begin{aligned}\sum_\mu e^{\frac{3\beta J}{2}Q_{\mu\mu}} = 3 &+ \frac{1}{2!}\left(\frac{3\beta J}{2}\right)^2 I_2 + \frac{1}{3!}\left(\frac{3\beta J}{2}\right)^3 I_3 + \frac{1}{4!}\left(\frac{3\beta J}{2}\right)^4 \frac{I_2^2}{2} + \frac{1}{5!}\left(\frac{3\beta J}{2}\right)^5 \frac{5}{6}I_2 I_3 \\ &+ \frac{1}{6!}\left(\frac{3\beta J}{2}\right)^6 \left(\frac{1}{4}I_2^3 + \frac{1}{3}I_3^2\right)\end{aligned} \tag{2.33}$$

The logarithm of this expression can be evaluated using the expansion

$$\ln(3+\delta) = \ln 3 + \left(\frac{\delta}{3}\right) - \frac{1}{2}\left(\frac{\delta}{3}\right)^2 + \frac{1}{3}\left(\frac{\delta}{3}\right)^3 - \frac{1}{4}\left(\frac{\delta}{3}\right)^4 + \frac{1}{5}\left(\frac{\delta}{3}\right)^5 - \frac{1}{6}\left(\frac{\delta}{3}\right)^6 + \cdots, \tag{2.34}$$

with $\delta = \ln\sum_\mu e^{\frac{3\beta J}{2}Q_{\mu\mu}} - 3$.

After straightforward but lengthy algebra, the Landau expansion of the free energy density takes the form

$$\begin{aligned}f = -\frac{\ln 3}{\beta J} + \frac{1}{2}\left(1 - \frac{3\beta J}{4}\right) I_2 - \frac{3(\beta J)^2}{16}I_3 + \frac{9(\beta J)^3}{256}I_2^2 + \frac{27(\beta J)^4}{512}I_2 I_3 \\ - \frac{117(\beta J)^5}{20480}I_2^3 + \frac{81(\beta J)^5}{5120}I_3^2\end{aligned} \tag{2.35}$$

Restricting attention to the uniaxial case and using the parametrization defined

in equation 1.6, the invariants reduce to

$$I_2 = \frac{3}{2}S^2, \quad I_3 = \frac{3}{4}S^3, \quad I_2^2 = \frac{9}{4}S^4, \quad I_2 I_3 = \frac{9}{8}S^5, \quad I_2^3 = \frac{27}{8}S^6, \quad I_3^2 = \frac{9}{16}S^6. \tag{2.36}$$

Introducing the reduced temperature $t = 1/(\beta J)$, equation 2.35 simplifies to

$$f = -t \ln 3 + \frac{3}{4}\left(1 - \frac{3}{4t}\right) S^2 - \frac{S^3}{4} + \frac{3}{16}S^4. \tag{2.37}$$

An analysis of equation 2.37 reveals the nature of the nematic–isotropic phase transition. The absence of a linear term in S allows for the existence of an isotropic phase with $S = 0$. In standard Landau theory, the coefficient of the quadratic term is written as $a(t-t^*)$ and determines the transition temperature. In the present case, the transition occurs in the vicinity of $t = 3/4$, which is the spinodal temperature of the isotropic phase. The presence of a negative cubic term in the expansion renders the transition first order, while the positive quartic term ensures thermodynamic stability.

CHAPTER 3

DILUTED MAIER–SAUPE MODEL

"Quand tu penses, ne sens-tu pas que
tu déranges secrètement quelque chose?"
Paul Valéry

The critical-like behavior of the nematic–isotropic (NI) phase transition remains a long-standing puzzle in the theoretical study of liquid crystals. Although it is well known that the NI transition is first order (DE GENNES and PROST (1993)), its small latent heat leads to large fluctuations that resemble those observed near the critical point of a continuous phase transition (SIMEAO and SIMOES (2013)). These pre-transitional fluctuations mimic critical behaviors and may be preempted by the first-order transition before a true critical regime is accessible (MUKHERJEE (1998)). Several studies have also investigated the possible existence of tricritical behavior in the vicinity of the NI transition (FRENKEL and EPPENGA (1982); WANG and KEYES (1996)).

Experimentally, the observation of these fluctuations is a difficult task. The first determination of the tricritical exponent for the NI transition was reported by KEYES and SHANE (1979). Later, LENART *et al.* (2012) obtained a value of $\beta = 0.28 \pm 0.03$ from nonlinear optical birefringence measurements in E7—this value supports the suggestion of tricritical behavior of the NI phase transition. At about the same time, SIMEAO and SIMOES (2013) proposed an alternative approach to evaluate the critical exponent β across all temperatures of the phase.

In the present chapter, the Maier–Saupe lattice model with dilution is employed to investigate the nature of the nematic–isotropic phase transition. This model is considered in light of the fact that the introduction of dilution is known to significantly modify the phase diagrams of many statistical models of physical interest (RODRIGUES *et al.* (2020)). A classic example is the emergence of a tricritical point in the annealed, site-diluted Ising model (AHARONY (1978); MARRO *et al.* (1986)). In statistical models, dilution elements represent the presence of inactive or non-interacting sites within the system, effectively introducing disorder into the underlying lattice. Physically, this can be interpreted as vacancies or impurities that do not contribute to the ordering mechanism.

In addition, experimental studies reporting tricritical behavior near the NI transition provide further motivation for investigating the diluted Maier-Saupe model. Furthermore, within the Landau–de Gennes framework, the free energy function can be expanded in the mean-field approximation, enabling the evaluation of the critical exponents near the transition and comparison with previous results.

3.1 Free Energy

The diluted Maier–Saupe model is defined, within the mean-field approximation, by the following Hamiltonian:

$$\mathcal{H} = -\frac{J}{2V}\sum_{i,j} t_i t_j \sum_{\mu,\nu} S_i^{\mu\nu} S_j^{\mu\nu}, \tag{3.1}$$

where $S_i^{\mu\nu} = \frac{3}{2} n_i^\mu n_i^\nu - \frac{1}{2}\delta_{\mu\nu}$ is a component of the order tensor expanded over the directions $\mu, \nu = x, y, z$, $t_i = 0, 1$ is the so-called occupation variable—$t_i = 1$ if the site is occupied and 0 otherwise—and V is the number of cells, with $\sum_{i=1}^{V} t_i = N$ being N the number of nematogens in the system. The switch from N to V in equation 3.1 is physically motivated because in the grand-canonical ensemble the constant N is not fixed. The connection between the two normalization constant is $J/V = (J/N)\cdot(N/V) = (J/N)\cdot\langle t\rangle$, where $\langle t\rangle = N/V$ is the mean occupation fraction. The undiluted limit is recovered when $\langle t\rangle \to 1$.

Working within the grand-canonical ensemble, it is assumed that the mixture of nematic and non-nematic sites is annealed. This means that the constituent particles are sufficiently mobile to reach thermal equilibrium on the timescale of the relevant experiments (AHARONY (1982)).

Under this assumption, the partition function must be written as

$$\Xi(\beta, \tilde{\mu}) = \sum_{N=0}^{V} e^{-\beta\tilde{\mu}N}\, \mathcal{Z}(\beta, N), \tag{3.2}$$

where $\beta = 1/k_B T$ and $\tilde{\mu}$ is the chemical potential which, for this analysis, it is considered negative[1].

To express $\Xi(\beta, \tilde{\mu})$ explicitly, it is convenient to first define the canonical partition function

$$\mathcal{Z} = \mathrm{Tr}'\exp(-\beta\mathcal{H}) = \sum_{\{t_i\}}{}' \sum_{\{\vec{n_i}\}} \exp\left(\frac{\beta J}{2V}\sum_{i,j} t_i t_j \sum_{\mu,\nu} S_i^{\mu\nu} S_j^{\mu\nu}\right), \tag{3.3}$$

[1]This choice restricts the physically accessible range of concentrations in the system. In the present work, positive values of the chemical potential are not considered.

where the prime symbol means a sum for a fixed N. Then

$$\Xi(\beta,\tilde{\mu}) = \sum_{\{t_i\}}{\sum_{\{\vec{n}_i\}}}' e^{-\beta\tilde{\mu}\sum_i t_i} \prod_{\mu,\nu} \exp\left[\frac{\beta J}{2V}\left(\sum_i t_i S_i^{\mu\nu}\right)^2\right]. \tag{3.4}$$

Note that the trace in the partition function is taken simultaneously over occupation variables t_i and molecular orientation $\{\vec{n}_i\}$.

The Hubbard–Stratonovich transformation is next introduced in order to decouple the random variables. In the present case, it takes the form:

$$e^{\frac{\beta J}{2V}\left(\sum_i t_i S_i^{\mu\nu}\right)^2} = \sqrt{\frac{V\beta J}{2\pi}} \int_{-\infty}^{+\infty} dQ_{\mu\nu} e^{-\frac{V\beta J}{2}Q_{\mu\nu}^2 + \beta J Q_{\mu\nu}\sum_i t_i S_i^{\mu\nu}}. \tag{3.5}$$

In the present case, it is required that $J > 0$.

By applying this transformation, the partition function becomes

$$\begin{aligned}\Xi &= \sum_{\{t_i\}}{\sum_{\{\vec{n}_i\}}}' e^{-\beta\tilde{\mu}\sum_i t_i} \prod_{\mu,\nu} \sqrt{\frac{V\beta J}{2\pi}} \int_{-\infty}^{+\infty} dQ_{\mu\nu} e^{-\frac{V\beta J}{2}Q_{\mu\nu}^2 + \beta J Q_{\mu\nu}\sum_i t_i S_i^{\mu\nu}} \\ &= \left[\prod_{\mu,\nu} \sqrt{\frac{V\beta J}{2\pi}} \int_{-\infty}^{+\infty} dQ_{\mu\nu} e^{-\frac{V\beta J}{2}Q_{\mu\nu}^2}\right] \{\boldsymbol{\Sigma}(t,\vec{n})\}^V. \end{aligned} \tag{3.6}$$

The model is further simplified by imposing the Zwanzig restriction: the vector $\vec{n}$ are restricted to the directions $\vec{n} = (\pm 1, 0, 0)$, $(0, \pm 1, 0)$, $(0, 0, \pm 1)$—which, according to DO CARMO *et al.* (2010), does not qualitatively alter the behavior of the system—the internal summation becomes:

$$\begin{aligned}\boldsymbol{\Sigma}(t,\vec{n}) = \sum_{\{t,\vec{n}\}} \exp\left[-\beta\tilde{\mu}t + \beta J \sum_{\mu,\nu} Q_{\mu\nu}\, t\left(\frac{3}{2}n^\mu n^\nu - \frac{1}{2}\delta_{\mu\nu}\right)\right] = 6 \\ + 2e^{-\beta\tilde{\mu}} \exp\left(-\frac{\beta J}{2}\sum_\mu Q_{\mu\mu}\right) \sum_\mu \exp\left(\frac{3}{2}\beta J\, Q_{\mu\mu}\right),\end{aligned}$$

which leads to

$$\begin{aligned}\Xi = \left[\prod_{\mu,\nu} \sqrt{\frac{V\beta J}{2\pi}} \int_{-\infty}^{+\infty} dQ_{\mu\nu} e^{-\frac{V\beta J}{2}Q_{\mu\nu}^2}\right] \\ \times \left\{6 + 2e^{-\beta\tilde{\mu}} \exp\left(-\frac{\beta J}{2}\sum_\mu Q_{\mu\mu}\right) \sum_\mu \exp\left(\frac{3}{2}\beta J Q_{\mu\mu}\right)\right\}^V.\end{aligned} \tag{3.7}$$

The grand canonical partition function can therefore be written as

$$\Xi(\beta,\tilde{\mu}) = \left[\prod_{\mu,\nu}\sqrt{\frac{V\beta J}{2\pi}}\int_{-\infty}^{+\infty} dQ_{\mu\nu}\right] e^{-\beta JV\phi(\beta,\tilde{\mu})}, \tag{3.8}$$

where

$$\phi(\beta,\tilde{\mu}) = \frac{1}{2}\sum_{\mu,\nu} Q_{\mu\nu}^2 - \frac{1}{\beta J}\ln\left[6 + 2e^{-\beta\tilde{\mu}}\exp\left(-\frac{\beta J}{2}\sum_{\mu} Q_{\mu\mu}\right)\sum_{\mu}\exp\left(\frac{3}{2}\beta J\, Q_{\mu\mu}\right)\right] \tag{3.9}$$

is the functional for the grand thermodynamical potential per lattice site. For the following derivations, the reduced temperature $t = 1/\beta J$ is defined, and $\tilde{\mu}/J \to \tilde{\mu}$.

3.2 Numerical Treatment

The integral in equation 3.8 can be approximated using the Saddle-Point method. In this approach, it is assumed that only the values of t and $\tilde{\mu}$ at which $\phi(t,\tilde{\mu})$ is a minimum contribute significantly to the integral. Starting from equation 3.9, the equations of state are obtained by imposing the stationary conditions

$$\frac{\partial\phi(t,\tilde{\mu})}{\partial Q_{\mu\nu}} = 0, \tag{3.10}$$

for each pair of directions μ,ν, in the large-V limit.

It is easy to see that if $\mu \neq \nu$, equation 3.10 yields

$$Q_{\mu\nu} = 0.$$

On the other hand, if $\mu = \nu$, the same condition leads to

$$S + \frac{1 - e^{\frac{9S}{4t}}}{2 + e^{\frac{9S}{4t}} + 3e^{\frac{S+4\tilde{\mu}}{4t}}} = 0, \tag{3.11}$$

where the parametrization $Q_{zz} \equiv S$, $Q_{yy} \equiv (\eta - S)/2$ and $Q_{xx} \equiv -(\eta + S)/2$ has been used, with $\eta = 0$. In the undiluted limit, it easy to see that equation 3.11 reduces to the standard Maier Saupe equation of state.

The stability of a given solution is determined from the Hessian matrix,

$$H = \begin{pmatrix} H_{11} & H_{12} & H_{13} \\ H_{12} & H_{11} & H_{13} \\ H_{13} & H_{13} & H_{33} \end{pmatrix}. \tag{3.12}$$

where the elements are obtained from second derivatives with respect to the variables

$Q_{\mu\mu}$, and the uniaxial parametrization $\eta = 0$ was taken. Explicitly,

$$
\begin{aligned}
H_{11} &= 1 - \frac{3\left(3 + 3e^{\frac{9S}{4t}} + 5e^{\frac{3S+4\tilde{\mu}}{4t}} + e^{\frac{3S+\tilde{\mu}}{t}}\right)}{4t\left(2 + e^{\frac{9S}{4t}} + 3e^{\frac{3S+4\tilde{\mu}}{4t}}\right)^2}, \\
H_{12} &= \frac{9 - 3e^{\frac{3S+4\tilde{\mu}}{4t}}\left(-4 + e^{\frac{9S}{4t}}\right)}{4t\left(2 + e^{\frac{9S}{4t}} + 3e^{\frac{3S+4\tilde{\mu}}{4t}}\right)^2}, \\
H_{13} &= \frac{9e^{\frac{9S}{4t}} + 3e^{\frac{3S+4\tilde{\mu}}{4t}} + 6e^{\frac{3S+\tilde{\mu}}{t}}}{4t\left(2 + e^{\frac{9S}{4t}} + 3e^{\frac{3S+4\tilde{\mu}}{4t}}\right)^2}, \\
H_{33} &= 1 - \frac{9e^{\frac{9S}{4t}} + 6e^{\frac{3S+\tilde{\mu}}{t}} + 3e^{\frac{3S+4\tilde{\mu}}{4t}}}{2t\left(2 + e^{\frac{9S}{4t}} + 3e^{\frac{3S+4\tilde{\mu}}{4t}}\right)^2}.
\end{aligned}
\tag{3.13}
$$

A solution characterized by specific values of t and $\tilde{\mu}$ is stable when all eigenvalues of H are positive. The spinodal limits are determined by analyzing the eigenvalues of the Hessian matrix for $S = 0$ (isotropic case) and $S \neq 0$ (nematic case).

Figure 3.1 shows the phase diagram in the t–$\tilde{\mu}$ plane, obtained by numerically solving equation 3.11. Two regions are identified: the uniaxial nematic phase (N) and the isotropic phase (I). The dashed lines represent the spinodal limits, whereas the solid black line marks the nematic–isotropic phase transition. Although this transition is first order, for values of $\tilde{\mu}$ close to zero it becomes weakly first order; this is reflected in the subtle variation of S, visible in the color scale, approaching the behavior of a second-order transition.

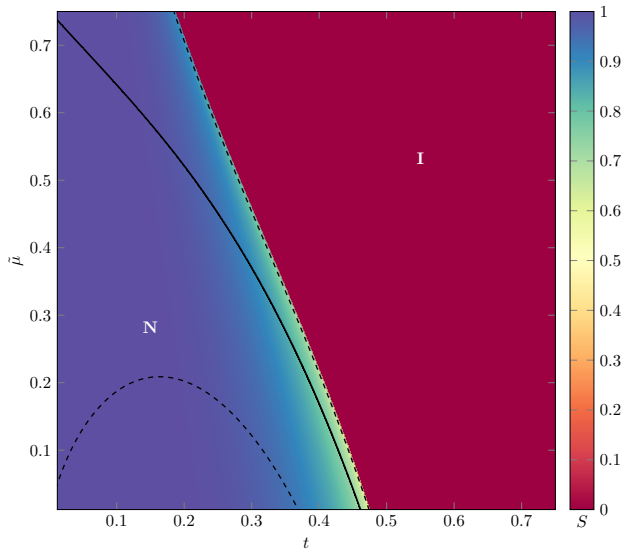

Figure 3.1: *Phase diagram for the diluted Maier-Saupe model in the $t - \tilde{\mu}$ plane. The color scale indicates the magnitude of the order parameter S at each point.*

3.3 A Landau–De Gennes Expansion Study

The basic assumption of the Landau–De Gennes (LG) theory is that for temperatures in the vicinity of the transition temperature the free-energy functional ϕ is an analytic function of the order parameter $\mathbf{Q}$ (DE GENNES and PROST (1993); GRAMSBERGEN *et al.* (1986)). In order to perform a Landau expansion for $\phi(\beta, \tilde{\mu})$ with respect to $\mathbf{Q}$, it is first necessary to construct all absolute rotational invariants, that is, all invariant combinations of the elements $Q_{\mu\nu}$. The most general invariant formed from $\mathbf{Q}$ has the form

$$I_m \equiv \operatorname{Tr} \mathbf{Q}^m = \sum_{\mu} Q_{\mu\mu}^m, \quad m = 1, 2, 3, \ldots . \tag{3.14}$$

An important property of any symmetric 3×3 matrix $\mathbf{Q}$, is that $\operatorname{Tr} \mathbf{Q}^m$ can be expressed as a polynomial in $\operatorname{Tr} \mathbf{Q}$, $\operatorname{Tr} \mathbf{Q}^2$ and $\operatorname{Tr} \mathbf{Q}^3$. Hence, up to sixth order,

$$I_4 = \frac{1}{2} I_2^2, \quad I_5 = \frac{5}{6} I_2 I_3, \quad \text{and} \quad I_6 = \frac{1}{4} I_2^3 + \frac{1}{3} I_3^2. \tag{3.15}$$

These expressions, together with the traceless condition of the order parameter, lead to a Landau expansion in terms of only $\operatorname{Tr} \mathbf{Q}^2$ and $\operatorname{Tr} \mathbf{Q}^3$.

In order to establish a connection with the LG expansion, it is necessary to expand the functional of the grand thermodynamic potential (equation 3.9) in terms of the rotational invariants introduced above. At first, note that

$$\begin{aligned} \sum_{\mu} e^{\frac{3Q_{\mu\mu}}{2t}} &= \sum_{\mu} \sum_{m=0}^{\infty} \frac{1}{m!} \left(\frac{3Q_{\mu\mu}}{2t} \right)^m = \sum_{m=0}^{\infty} \frac{1}{m!} \left(\frac{3}{2t} \right)^m \sum_{\mu} Q_{\mu\mu}^m = \sum_{m=0}^{\infty} \frac{1}{m!} \left(\frac{3}{2t} \right)^m I_m \\ &= 3 + \frac{1}{2!} \left(\frac{3}{2t} \right)^2 I_2 + \frac{1}{3!} \left(\frac{3}{2t} \right)^3 I_3 + \frac{1}{4!} \left(\frac{3}{2t} \right)^4 I_4 + \frac{1}{5!} \left(\frac{3}{2t} \right)^5 I_5 + \cdots . \end{aligned}$$

Expanding to the 6th term, and using 3.15, one obtains

$$\begin{aligned} \sum_{\mu} e^{\frac{3Q_{\mu\mu}}{2t}} = 3 + \frac{1}{2!} \left(\frac{3}{2t} \right)^2 I_2 + \frac{1}{3!} \left(\frac{3}{2t} \right)^3 I_3 + \frac{1}{4!} \left(\frac{3}{2t} \right)^4 \frac{I_2^2}{2} + \frac{1}{5!} \left(\frac{3}{2t} \right)^5 \frac{5}{6} I_2 I_3 \\ + \frac{1}{6!} \left(\frac{3}{2t} \right)^6 \left(\frac{1}{4} I_2^3 + \frac{1}{3} I_3^2 \right) + \cdots . \end{aligned}$$

Additionally,

$$\exp\left(-\frac{1}{2t} \sum_{\mu} Q_{\mu\mu} \right) = 1,$$

because the traceless condition implies $\sum_\mu Q_{\mu\mu} = 0$. Using the relations above,

$$\ln\left[3+e^{-\frac{\tilde{\mu}}{t}}\sum_\mu e^{\frac{3Q_{\mu\mu}}{2t}}\right] = \ln\left[3+e^{-\frac{\tilde{\mu}}{t}}\left(3+\frac{1}{2!}\left(\frac{3}{2t}\right)^2 I_2+\frac{1}{3!}\left(\frac{3}{2t}\right)^3 I_3+\frac{1}{4!}\left(\frac{3}{2t}\right)^4\frac{I_2^2}{2}\right.\right.$$
$$\left.\left.+\frac{1}{5!}\left(\frac{3}{2t}\right)^5\frac{5}{6}I_2I_3+\frac{1}{6!}\left(\frac{3}{2t}\right)^6\left(\frac{1}{4}I_2^3+\frac{1}{3}I_3^2\right)+\cdots\right)\right],$$

This expression can be rewritten as

$$\ln\left[3+3e^{-\frac{\tilde{\mu}}{t}}+e^{-\frac{\tilde{\mu}}{t}}\xi\right] = \ln\left[\xi+e^{-\frac{\tilde{\mu}}{t}}\Phi\right], \tag{3.16}$$

where $\xi = 3+3e^{-\frac{\tilde{\mu}}{t}}$ and

$$\Phi = \frac{1}{2!}\left(\frac{3}{2t}\right)^2 I_2+\frac{1}{3!}\left(\frac{3}{2t}\right)^3 I_3+\frac{1}{4!}\left(\frac{3}{2t}\right)^4\frac{I_2^2}{2}+\frac{1}{5!}\left(\frac{3}{2t}\right)^5\frac{5}{6}I_2I_3+\frac{1}{6!}\left(\frac{3}{2t}\right)^6\left(\frac{1}{4}I_2^3+\frac{1}{3}I_3^2\right)+\cdots.$$

Expanding the logarithm yields

$$\ln\left[\xi+e^{-\frac{\tilde{\mu}}{t}}\Phi\right] = \ln\xi+\left(\frac{e^{-\frac{\tilde{\mu}}{t}}\Phi}{\xi}\right)-\frac{1}{2}\left(\frac{e^{-\frac{\tilde{\mu}}{t}}\Phi}{\xi}\right)^2+\frac{1}{3}\left(\frac{e^{-\frac{\tilde{\mu}}{t}}\Phi}{\xi}\right)^3-\frac{1}{4}\left(\frac{e^{-\frac{\tilde{\mu}}{t}}\Phi}{\xi}\right)^4+\cdots,$$

and retaining only terms up to sixth order in $Q_{\mu\mu}$,

$$\ln\left[\xi+e^{-\frac{\tilde{\mu}}{t}}\Phi\right] = \ln\xi+\frac{e^{-\frac{\tilde{\mu}}{t}}}{\xi}\left[\frac{1}{2!}\left(\frac{3}{2t}\right)^2 I_2+\frac{1}{3!}\left(\frac{3}{2t}\right)^3 I_3+\frac{1}{4!}\left(\frac{3}{2t}\right)^4\frac{I_2^2}{2}\right.$$
$$\left.+\frac{1}{5!}\left(\frac{3}{2t}\right)^5\frac{5}{6}I_2I_3+\frac{1}{6!}\left(\frac{3}{2t}\right)^6\left(\frac{1}{4}I_2^3+\frac{1}{3}I_3^2\right)\right]$$
$$-\frac{e^{-\frac{2\tilde{\mu}}{t}}}{2\xi^2}\left[\frac{1}{(2!)^2}\left(\frac{3}{2t}\right)^4 I_2^2+\frac{2}{3!\cdot 2!}\left(\frac{3}{2t}\right)^5 I_2I_3+\frac{1}{4!\cdot 2!}\left(\frac{3}{2t}\right)^6 I_2^3\right.$$
$$\left.+\frac{1}{(3!)^2}\left(\frac{3}{2t}\right)^6 I_3^2\right]+\frac{e^{-\frac{3\tilde{\mu}}{t}}}{3\xi^3}\left[\frac{1}{(2!)^3}\left(\frac{3}{2t}\right)^6 I_2^3\right].$$

After straightforward algebraic simplification, the result is

$$\ln\left[\xi+e^{-\frac{\tilde{\mu}}{t}}\Phi\right] = \ln\xi+\frac{3^2}{2^3t^2}\frac{e^{-\frac{\tilde{\mu}}{t}}}{\xi}I_2+\frac{3^2}{2^4t^3}\frac{e^{-\frac{\tilde{\mu}}{t}}}{\xi}I_3+\frac{e^{-\frac{\tilde{\mu}}{t}}}{\xi}\left(\frac{3^3}{2^8t^4}-\frac{3^4}{2^7t^4}\frac{e^{-\frac{\tilde{\mu}}{t}}}{\xi}\right)I_2^2$$
$$+\frac{e^{-\frac{\tilde{\mu}}{t}}}{\xi}\left(\frac{3^3}{2^9t^5}-\frac{3^4}{2^7t^5}\frac{e^{-\frac{\tilde{\mu}}{t}}}{\xi}\right)I_2I_3+\frac{e^{-\frac{\tilde{\mu}}{t}}}{\xi}\left(\frac{3^4}{5\cdot 2^{12}t^6}-\frac{3^5}{2^{11}t^6}\frac{e^{-\frac{\tilde{\mu}}{t}}}{\xi}+\frac{3^5}{2^9t^6}\frac{e^{-\frac{2\tilde{\mu}}{t}}}{\xi^2}\right)I_2^3$$
$$+\frac{e^{-\frac{\tilde{\mu}}{t}}}{\xi}\left(\frac{3^3}{5\cdot 2^{10}t^6}-\frac{3^4}{2^9t^6}\frac{e^{-\frac{\tilde{\mu}}{t}}}{\xi}\right)I_3^2.$$

Finally, the free-energy functional expressed in terms of the invariants I_m is

$$\phi(t,\tilde{\mu},I_m) = -t\ln\xi - \left(\frac{3^2}{2^3 t}\frac{e^{-\frac{\tilde{\mu}}{t}}}{\xi} - \frac{1}{2}\right) I_2 - \frac{3^2}{2^4 t^2}\frac{e^{-\frac{\tilde{\mu}}{t}}}{\xi} I_3 - \frac{e^{-\frac{\tilde{\mu}}{t}}}{\xi}\left(\frac{3^3}{2^8 t^3} - \frac{3^4}{2^7 t^3}\frac{e^{-\frac{\tilde{\mu}}{t}}}{\xi}\right) I_2^2$$
$$- \frac{e^{-\frac{\tilde{\mu}}{t}}}{\xi}\left(\frac{3^3}{2^9 t^4} - \frac{3^4}{2^7 t^4}\frac{e^{-\frac{\tilde{\mu}}{t}}}{\xi}\right) I_2 I_3 - \frac{e^{-\frac{\tilde{\mu}}{t}}}{\xi}\left(\frac{3^4}{5\cdot 2^{12} t^5} - \frac{3^5}{2^{11} t^5}\frac{e^{-\frac{\tilde{\mu}}{t}}}{\xi} + \frac{3^5}{2^9 t^5}\frac{e^{-\frac{2\tilde{\mu}}{t}}}{\xi^2}\right) I_2^3$$
$$- \frac{e^{-\frac{\tilde{\mu}}{t}}}{\xi}\left(\frac{3^3}{5\cdot 2^{10} t^5} - \frac{3^4}{2^9 t^5}\frac{e^{-\frac{\tilde{\mu}}{t}}}{\xi}\right) I_3^2. \quad (3.17)$$

The equation 3.17 can be expressed as

$$\phi = \phi_0 + \frac{a}{2} I_2 + \frac{b}{3} I_3 + \frac{c}{4} I_2^2 + \frac{d}{5} I_2 I_3 + \frac{e}{6} I_2^3 + \frac{e'}{6} I_3^2, \quad (3.18)$$

where the coefficients are given by

$$a = -\left(\frac{3^2}{2^2 t}\frac{e^{-\frac{\tilde{\mu}}{t}}}{\xi} - 1\right) = -\left(\frac{3}{4t} g - 1\right),$$
$$b = -\frac{3^3}{2^4 t^2}\frac{e^{-\frac{\tilde{\mu}}{t}}}{\xi} = -\frac{9}{16 t^2} g,$$
$$c = -\frac{e^{-\frac{\tilde{\mu}}{t}}}{\xi}\left(\frac{3^3}{2^6 t^3} - \frac{3^4}{2^5 t^3}\frac{e^{-\frac{\tilde{\mu}}{t}}}{\xi}\right) = -\frac{3^2 g}{2^5 t^3}\left(\frac{1}{2} - g\right),$$
$$d = -\frac{5 e^{-\frac{\tilde{\mu}}{t}}}{\xi}\left(\frac{3^3}{2^9 t^4} - \frac{3^4}{2^7 t^4}\frac{e^{-\frac{\tilde{\mu}}{t}}}{\xi}\right) = -\frac{3^2 g}{2^5 t^3}\left(\frac{1}{4} - g\right),$$
$$e = -\frac{e^{-\frac{\tilde{\mu}}{t}}}{\xi}\left(\frac{3^5}{5\,2^{11} t^5} - \frac{3^6}{2^{10} t^5}\frac{e^{-\frac{\tilde{\mu}}{t}}}{\xi} + \frac{3^6}{2^8 t^5}\frac{e^{-2\frac{\tilde{\mu}}{t}}}{\xi}\right) = -\frac{3^4 g}{5\,2^8 t^5}\left(\frac{1}{2^3} - \frac{5}{2^2} g + \frac{5}{3} g^2\right), \text{ and}$$
$$e' = -\frac{e^{-\frac{\tilde{\mu}}{t}}}{\xi}\left(\frac{3^3}{5\cdot 2^{10} t^5} - \frac{3^4}{2^9 t^5}\frac{e^{-\frac{\tilde{\mu}}{t}}}{\xi}\right) = -\frac{3^2 g}{5\,2^9 t^5}\left(\frac{1}{2} - 5\,g\right), \quad (3.19)$$

with,

$$g = \frac{1}{1 + e^{\frac{\tilde{\mu}}{t}}}. \quad (3.20)$$

In order to make connection with experiments, it is convenient to express the equation 3.18 in terms of the quantity S. The order parameter tensor is

$$\mathcal{Q} = \begin{pmatrix} -\frac{1}{2}(S+\eta) & 0 & 0 \\ 0 & -\frac{1}{2}(S-\eta) & 0 \\ 0 & 0 & S \end{pmatrix}, \quad (3.21)$$

in the uniaxial case, it leads to the following invariants:

$$I_2 = \frac{3}{2}S^2, \quad I_3 = \frac{3}{4}S^3, \quad I_2^2 = \frac{9}{4}S^4, \quad I_2 I_3 = \frac{9}{8}S^5, \quad I_2^3 = \frac{27}{8}S^6, \quad I_3^2 = \frac{9}{16}S^6. \tag{3.22}$$

Substituting these expressions into the free energy, yields

$$\phi(t, g, S) = \phi_0 + AS^2 + BS^3 + CS^4 + DS^5 + ES^6 + E'S^6, \tag{3.23}$$

where

$$A = \frac{3}{4}\left(1 - \frac{3g}{4t}\right), \quad B = -\frac{9g}{64t^2}, \quad C = \frac{9g}{2^7 t^3}\left(g - \frac{1}{2}\right), \quad D = \frac{3^4 g}{2^{10} t^4}\left(g - \frac{1}{4}\right),$$
$$E = \frac{3^6 g}{5\,2^{12} t^5}\left(\frac{5}{4}g - \frac{5}{3}g^2 - \frac{1}{8}\right), \text{ and } \quad E' = \frac{3^3 g}{5\,2^{12} t^5}\left(5\,g - \frac{1}{2}\right). \tag{3.24}$$

From the general expansion in equation 3.23, conclusions regarding the phase transition can be drawn.

3.4 Landau–De Gennes Phase Diagram and Critical Behavior

Restrictions on the coefficients of the expansion arise from symmetry considerations. In equation 3.23, the equilibrium values of S are obtained by minimizing ϕ with respect to S, i.e.,

$$\frac{\partial \phi}{\partial S} = 0 \text{ and } \frac{\partial^2 \phi}{\partial S^2} = 0. \tag{3.25}$$

The requirement that ϕ describe a phase transition between states with distinct values of S, together with the existence of a spinodal—the point at which a phase loses stability—in a first-order phase transition, implies that A must change sign as a function of t and g. Consequently, the coefficient A is assumed to have the form $A = a(t - t^*)$, where a is a constant and t^* is a temperature close to the NI transition. The presence of a small cubic term in equation 3.23 results in a small entropy jump, rendering the transition close to second order (MUKHERJEE (1998)). If $B = 0$, the temperature t^* would coincide with the mean-field second order transition temperature. However, since $B < 0$ in the present model, t^* corresponds to the temperature marking the absolute stability limit of the isotropic phase, i.e., the isotropic spinodal. The spinodal is therefore determined by the condition $A(t, g) = 0$, which defines a line in the $t - g$ phase diagram (Figure 3.2).

3.4.1 Fourth Order Expansion

When $C > 0$—a condition satisfied for $g > 1/2$— the relation 3.23 can be written as

$$\phi(t, g, S) = \phi_0 + AS^2 + BS^3 + CS^4. \tag{3.26}$$

The stability conditions in equation 3.25 leads to the following system of equations:

$$\begin{cases} 2A + 3BS + 4CS^2 = 0 \\ 2A + 6BS + 12CS^2 = 0 \end{cases} \implies S = -\frac{3B}{8C} \text{ and } A = \frac{9B^2}{32C}. \tag{3.27}$$

Also, from the requirement that the isotropic and nematic phases have equal free energy along the transition line it follows that

$$\begin{cases} 2A + 3BS + 4CS^2 = 0 \\ A + BS + CS^2 = 0 \end{cases} \implies S = -\frac{B}{2C} \text{ and } A = \frac{B^2}{4C}. \tag{3.28}$$

By substituting the coefficients given in equation 3.24, equations 3.28 and 3.27 yield, respectively, the nematic spinodal line and the nematic–isotropic phase transition line in the $t - g$ plane, as shown in figure 3.2. Considering that the temperature dependence appears only in the first term, as stated above, the spinodal temperatures of the Nematic phase and the NI transition curve follows from equations 3.28 and 3.27 respectively as

$$t^\dagger = t^* + \frac{9B^2}{32a\,C} \text{ and } \quad t_{NI} = t^* + \frac{B^2}{4a\,C}. \tag{3.29}$$

The corresponding information is displayed in the phase diagram shown in Figure 3.2. The red and blue dashed lines indicate the spinodal boundaries of the isotropic and nematic phases, respectively, while the solid black line represents the nematic–isotropic phase transition. It is important to note that this analysis is valid only for $C > 0$, i.e., $g > 1/2$. For $g < 1/2$ (gray region), additional terms are required to stabilize the expansion in equation 3.23; this extension will be addressed in the next subsection.

3.4.2 Effective Tricritical point

The existence of multicritical points is characterized when two coefficients of the same symmetry in the Landau free energy vanish simultaneously (GRAMSBERGEN *et al.* (1986)). Particularly, a tricritical point occurs when A and C are equal to zero. In the phase diagram, this situation corresponds to the intersection of a line of first-order phase transitions with a line of second-order phase transitions. In the

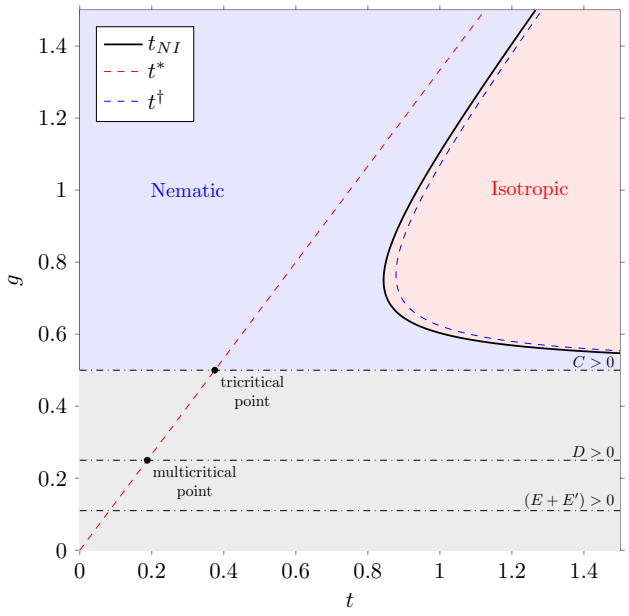

Figure 3.2: *Diluted Maier–Saupe model in the t–g plane. Effective tricritical behavior occurs at $A = C = 0$. The lines t^*, $t^\dagger$, and t_{NI} correspond to the isotropic spinodal, nematic spinodal, and phase transition line, respectively.*

expansion, a tricritical effective condition is reached when $A = C = 0$, with $D > 0$. Setting $C = 0$[2] in equation 3.23 gives the reduced expansion

$$\phi(t, g, S) = AS^2 + BS^3 + DS^5, \tag{3.30}$$

where a stabilizing term $D > 0$ must be added— which is satisfied for $g > 1/4$. Under these conditions, the spinodal temperatures of the Nematic phase and the NI transition curve are

$$t^\dagger = t^* - \frac{4}{3\sqrt{3}\,a}\left(-\frac{B^3}{D}\right)^{1/2} \quad \text{and} \quad t_{NI} = t^* - \frac{14\sqrt{5}}{27\,a}\left(-\frac{B^3}{D}\right)^{1/2}. \tag{3.31}$$

At these temperatures, the corresponding order parameters are

$$S^\dagger = \frac{1}{\sqrt{3}}\sqrt{-\frac{B}{D}} \quad \text{and} \quad S_{NI} = \frac{\sqrt{5}}{3}\sqrt{-\frac{B}{D}}. \tag{3.32}$$

The equilibrium condition for S is then given by

$$(S - S^\dagger)^3 + 3S^\dagger(S - S^\dagger)^2 - \frac{a}{D}(t - t^\dagger) = 0. \tag{3.33}$$

From equation 3.33, the temperature dependence of the scalar order parameter can be expressed as

$$(S - S^\dagger) \sim (t - t^\dagger)^{\beta_c}. \tag{3.34}$$

[2]In the original variables $(t, \tilde{\mu})$, the tricritical condition $C = 0$ renders $\tilde{\mu} = 0$.

For the case where $C = 0$ and $B \neq 0$, the critical exponent is $\beta_c = 1/2$. If $B = 0$, then $S^\dagger = 0$ and equation 3.33 yields $\beta_c = 1/3$. Although the condition for $B = 0$ represents a theoretical impossibility, experimentally if B is very small around the transition point, quasi-tricritical behavior with $\beta_c \approx 1/3$ can be observed, in consonance with experimental results obtained by LENART *et al.* (2012).

3.4.3 Higher-order multicritical points

To explore the phase behavior in the gray area in figure 3.2 it is necessary to consider additional stabilizing terms in the expression. In the case where $D = C = 0$, equation 3.23 becomes

$$\phi(t, g, S) = AS^2 + BS^3 + (E + E')S^6, \tag{3.35}$$

where the stabilizing term $(E + E') > 0$ is included. By following the same procedures, the nematic spinodal and the NI transition line is given respectively by

$$t^\dagger = t^* + \frac{7}{63^{2/3}} \frac{E + E'}{a} \left(-\frac{B}{(E + E')} \right)^{4/3} \quad \text{and} \quad t_{NI} = t^* + \frac{3}{42^{2/3}} \frac{E + E'}{a} \left(-\frac{B}{(E + E')} \right)^{4/3}. \tag{3.36}$$

Several observations follow from this analysis. For $g > 1/2$, the lowest-order terms in the Landau expansion dominate the behavior of the system, and the temperatures defined in equation 3.29 fully characterize the phase transition and the stability of the ordered phase. Upon entering the gray region, the phase exhibits a richer behavior. For $g > 1/4$, the D-term in the expansion is positive and stabilizes the solution; in this regime, the temperatures defined in 3.31 determine the transition boundaries. Finally, for $g > 0.11$, the last two terms in the expansion provide the dominant stabilizing contribution, and the system behavior is described by equation 3.36.

CHAPTER 4

FERROELECTRIC NEMATIC LIQUID-CRYSTALLINE PHASES

"Tenho um pouco de medo: medo ainda de me entregar pois o próximo instante é o desconhecido. O próximo instante é feito por mim? ou se faz sozinho?"
Clarice Lispector

In 1916, Max Born predicted the existence of a ferroelectric fluid in which all the molecular dipoles point in the same direction. However, it took over a century to find solid experimental evidence for such a state. Research in this field was revolutionized in 2017 when two groups independently reported novel nematic phases in strongly dipolar mesogens. Particularly, a new nematic phase was observed in the compound RM734 (MERTELJ *et al.* (2018))—later demonstrated to be ferronematic by CHEN *et al.* (2020)—, while a *ferroelectric-like* nematic phase was reported in the compound DIO (NISHIKAWA *et al.* (2017)). In both systems, the constituent molecules were rod-like and contained multiple intramolecular dipoles distributed along their length, whose projections onto the molecular long axis combined to produce a large net axial dipole moment. The discovery of the ferroelectric nematic phase (N_F) has expanded into what researchers calls the **Ferroelectric Nematic Realm**, at which a collection of related phases including Chiral Ferroelectric Nematic, Antiferroelectric Smectic Z, and Ferroelectric Smectic A are included (CHEN (2024)).

Recent experimental observation of the N_F phase have motivated the application of Landau–de Gennes-type models to characterize the symmetry breaking associated with the transition from non-polar to polar states. For example, MERTELJ *et al.* (2018) argued that "a Landau–de Gennes type of phenomenological theory can be used to describe the phase transition in the RM734 molecule". In parallel, extensions of the Maier–Saupe theory incorporating dipolar interaction terms in the mean-field potential have also played an important role in advancing theoretical understanding of these systems (ETXEBARRIA *et al.* (2022)).

The purpose of the present chapter is to provide a concise overview of the experimental perspectives reported in the literature on this rapidly developing field,

as well as to investigate modifications of the Maier–Saupe model that account for dipolar interactions at the molecular level that mimic the dipolar electric interaction on ferroelectric nematic phases.

4.1 Ferroelectric Nematic Realm

In the conventional nematic phase, the principal molecular axis—which posses inversion symmetry— are, on average, oriented about a common vector known as the director, denoted by a unit vector $\tilde{\mathbf{N}}$. This symmetry demands an apolar interaction between the nematic molecules. The order parameter is mathematically described as a traceless second-rank tensor, known as the nematic order parameter, with components defined as

$$\mathcal{Q}^{\mu\nu} = S\Big(\frac{3}{2}n^{\mu}n^{\nu} - \frac{1}{2}\delta_{\mu\nu}\Big), \tag{4.1}$$

where n^{μ} and n^{ν} denote the components of the local molecular orientation, and S is the scalar order parameter that quantifies how well the molecules are oriented along $\tilde{\mathbf{N}}$. The macroscopic behavior of this phase is strongly influenced by the anisotropic shape of the constituent molecules.

In the ferronematic phase, by contrast, inversion symmetry of the order parameter is broken. In this case, the dominant ordering mechanism arises from interactions between molecular electric dipoles, and the resulting phase exhibits a spontaneous, nonzero polarization density.

4.1.1 Experimental Phenomenology

The first solid experimental evidence for a ferronematic phase was reported by MERTELJ *et al.* (2018), who showed that the low-temperature nematic phase of the polar rod-like compound RM734—characterized by a large molecular dipole moment—undergoes a weakly first-order transition to a new phase in which the director develops a periodic splay modulation rather than remaining spatially homogeneous. In that work, a novel phase termed the *splay nematic phase* (N_S) was proposed and characterized by a distinctive modulated structure driven by molecular shape. Polarization microscopy images comparing the nematic and N_S phases revealed the emergence of additional defect lines in the latter, indicating a lower symmetry than that of the conventional nematic phase. Furthermore, dynamic light-scattering measurements showed pronounced pre-transitional splay modulations of the elastic constants, in contrast to ordinary nematic, for which elastic constants are generally stable and follow universal power laws associated with the order parameter

SIMÕES *et al.* (2013).

Later, CHEN *et al.* (2020) showed that the low-temperature phase on the RM734 compound exhibits all the characteristics expected from a ferronematic phase. The authors claimed that by observation of the electro-optic behavior of RM734 using polarized light they obtained no evidence for a splay nematic phase but rather the strong conclusion that upon cooling from higher-temperature the material undergoes a transition from nematic to another uniaxial nematic phase that is ferroelectric. The principal evidence supporting this conclusion is the observation, in a nematic liquid crystal, of the defining features of ferroelectricity: (i) the spontaneous formation of polar domains with opposite polarization in the absence of an applied electric field, separated by well-defined domain boundaries, and (ii) electric-field-induced polarization reversal mediated by the motion of these domain boundaries, as illustrated in Figure 4.1.

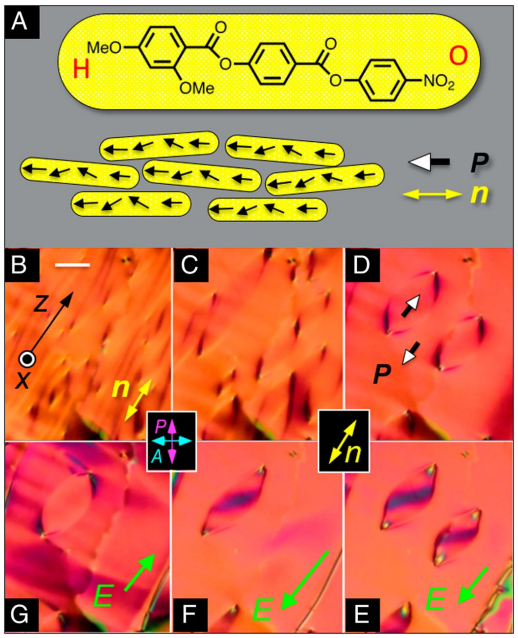

Figure 4.1: *Ferroelectric nematic phase. (A) Structure of RM734 compound and schematic of molecular alignment in the ferroelectric nematic phase. (B-E) electro-optic evidence for ferroelectricity in the N_F phase. Adapted from CHEN (2024) under CC BY-NC 4.0.*

Independently, NISHIKAWA *et al.* (2017) reported a liquid-crystal compound, DIO, composed of elongated molecules possessing a nonzero internal dipole moment, which exhibits ferroelectric-like polar order in a phase that was previously expected to be nematic. Within the temperature range where this phase is observed, the dielectric permittivity becomes extraordinarily large—several hundred times greater than that of conventional nematic phases. According to the authors, *"the remarkably large dielectric permittivity cannot be explained by a simple nematic order in which the statistical distribution of molecular head–tail directions along the director*

is even and there is no macroscopic dipole (...). Thus, it is reasonable to conclude that there should be a ferroelectric-like order of the phase.". In addition, simultaneous observations using polarized optical microscopy revealed a sandy, multi-domain texture that is absent in conventional nematics. This texture is consistent with a reorientation of the director and the formation of large ensembles of polar domains, a mechanism that naturally leads to a strong macroscopic ferroelectric-like polarization.

In this context, the available experimental evidence for the ferronematic phase is sufficiently compelling to motivate theoretical studies aimed at extending classical models to account for this extraordinary new phase.

4.2 Ferroelectric Maier-Saupe Extension

Inspired by ETXEBARRIA *et al.* (2022), the proposed Maier–Saupe Hamiltonian includes an additional term accounting for dipolar interactions and is written as

$$\mathcal{H} = -A \sum_{\langle i,j \rangle} \mathbf{S}_i : \mathbf{S}_j - B \sum_{\langle i,j \rangle} \mathbf{n}_i \cdot \mathbf{n}_j, \tag{4.2}$$

where A and B are the nematic and polar (dipolar) coupling constants, respectively, and $\langle : \rangle$ is the Frobenius inner product.

4.2.1 Free Energy

Within the mean-field approximation, the Hamiltonian of equation 4.2 takes the form

$$\mathcal{H} = -\frac{A}{2N} \sum_{i,j} \sum_{\mu,\nu} S_i^{\mu\nu} S_j^{\mu\nu} - \frac{B}{2N} \sum_{i,j} \sum_{\mu,\nu} n_i^\mu n_j^\nu \delta_{\mu\nu}, \tag{4.3}$$

where $S_i^{\mu\nu} = \frac{3}{2} n_i^\mu n_i^\nu - \frac{1}{2}\delta_{\mu\nu}$ denotes a component of the tensor order parameter defined over the Cartesian directions $(\mu, \nu) = x, y, z$. The Kronecker delta $\delta_{\mu\nu}$ is included in the second term to ensure symmetry.

The canonical partition function is then given by

$$\begin{aligned} \mathcal{Z} = \operatorname{Tr} \exp(-\beta \mathcal{H}) &= \operatorname{Tr} \exp\left(\frac{\beta A}{2N} \sum_{i,j} \sum_{\mu,\nu} S_i^{\mu\nu} S_j^{\mu\nu} + \frac{\beta B}{2N} \sum_{i,j} \sum_{\mu,\nu} n_i^\mu n_j^\nu \delta_{\mu\nu} \right) \\ &= \operatorname{Tr} \prod_{\mu,\nu} \exp\left(\frac{\beta A}{2N} \sum_{i,j} S_i^{\mu\nu} S_j^{\mu\nu} + \frac{\beta B}{2N} \sum_{i,j} n_i^\mu n_j^\nu \delta_{\mu\nu} \right). \end{aligned} \tag{4.4}$$

Noting that

$$\sum_{i,j} S_i^{\mu\nu} S_j^{\mu\nu} = \left(\sum_i S_i^{\mu\nu} \right)^2 \quad \text{and} \quad \sum_{i,j} n_i^\mu n_j^\nu \delta_{\mu\nu} = \left(\sum_i n_i^\mu \delta_{\mu\nu} \right)^2 ,$$

the partition function may be rewritten as

$$\mathcal{Z} = \mathrm{Tr} \prod_{\mu,\nu} \exp \left[\frac{\beta A}{2N} \left(\sum_i S_i^{\mu\nu} \right)^2 + \frac{\beta B}{2N} \left(\sum_i n_i^\mu \delta_{\mu\nu} \right)^2 \right] . \tag{4.5}$$

At this stage, the Hubbard–Stratonovich transformation is introduced[1]. In the present case, it reads:

$$e^{\frac{\beta A}{2N} \left(\sum_i S_i^{\mu\nu} \right)^2} = \sqrt{\frac{N\beta A}{2\pi}} \int_{-\infty}^{+\infty} dQ_{\mu\nu} e^{-\frac{N\beta A}{2} Q_{\mu\nu}^2 + \beta A Q_{\mu\nu} \sum_i S_i^{\mu\nu}} ; \tag{4.6}$$

and

$$e^{\frac{\beta B}{2N} \left(\sum_i n_i^\mu \delta_{\mu\nu} \right)^2} = \sqrt{\frac{N\beta B}{2\pi}} \int_{-\infty}^{+\infty} dM_{\mu\nu} e^{-\frac{N\beta B}{2} M_{\mu\nu}^2 + \beta B M_{\mu\nu} \sum_i n_i^\mu \delta_{\mu\nu}} . \tag{4.7}$$

It is important to note that $M_{\mu\nu}$ is effectively diagonal—i.e., $M_{\mu\nu} = M_\mu \delta_{\mu\nu}$—and thus represents a polar vector.

The partition function thus becomes

$$\begin{aligned} \mathcal{Z} &= \mathrm{Tr} \prod_{\mu,\nu} \frac{N\beta}{2\pi} \sqrt{AB} \int_{-\infty}^{+\infty} dQ_{\mu\nu} dM_{\mu\nu} e^{-\frac{N\beta A}{2} Q_{\mu\nu}^2 + \beta A Q_{\mu\nu} \sum_i S_i^{\mu\nu}} e^{-\frac{N\beta B}{2} M_{\mu\nu}^2 + \beta B M_{\mu\nu} \sum_i n_i^\mu \delta_{\mu\nu}} \\ &= \left[\prod_{\mu,\nu} \frac{N\beta}{2\pi} \sqrt{AB} \int_{-\infty}^{+\infty} dQ_{\mu\nu} dM_{\mu\nu} e^{-\frac{N\beta A}{2} Q_{\mu\nu}^2 - \frac{N\beta B}{2} M_{\mu\nu}^2} \right] \mathrm{Tr}\, K_{xy}, \end{aligned} \tag{4.8}$$

where

$$\mathrm{Tr}\, K_{xy} = \sum_{\{\vec{n}\}} \exp \left[\beta A \sum_i \sum_{\mu,\nu} Q_{\mu\nu} S_i^{\mu\nu} + \beta B \sum_i \sum_{\mu,\nu} M_{\mu\nu} n_i^\mu \delta_{\mu\nu} \right] .$$

Assuming the Zwanzig discretization, $\vec{n} = (\pm 1, 0, 0); (0, \pm 1, 0); (0, 0, \pm 1)$, and considering N independent molecules, one finds

$$\mathrm{Tr}\, K_{xy} = \left(2 e^{-\frac{\beta A}{2} \sum_\mu Q_{\mu\mu}} \sum_\mu e^{\frac{3}{2t} \beta A Q_{\mu\mu}} \cosh \left(\beta B M_{\mu\mu} \right) \right)^N . \tag{4.9}$$

[1] In this case, the HS transformation requires $B > 0$, given that $B < 0$ would correspond to an antiferrroelectric interaction

The full partition function can therefore be written as

$$\mathcal{Z} = \left[\prod_{\mu,\nu} \frac{N\beta}{2\pi}\sqrt{AB}\int_{-\infty}^{+\infty} dQ_{\mu\nu}dM_{\mu\nu}e^{-\frac{N\beta A}{2}Q_{\mu\nu}^2-\frac{N\beta B}{2}M_{\mu\nu}^2}\right] \times \left(2e^{-\frac{\beta A}{2}\sum_\mu Q_{\mu\mu}}\sum_\mu e^{\frac{3}{2}\beta A Q_{\mu\mu}}\cosh\left(\beta B M_{\mu\mu}\right)\right)^N, \quad (4.10)$$

and is convenient to write

$$\mathcal{Z} = \left[\prod_{\mu,\nu} \frac{N\beta}{2\pi}\sqrt{AB}\int_{-\infty}^{+\infty} dQ_{\mu\nu}dM_{\mu\nu}\right] e^{-N\beta\mathcal{F}(Q_{\mu\nu},M_{\mu\nu})}, \quad (4.11)$$

with $N \to \infty$, and

$$\mathcal{F}(Q_{\mu\nu},M_{\mu\nu}) = \frac{1}{2}\sum_{\mu,\nu}Q_{\mu\nu}^2+\frac{B}{2A}\sum_{\mu,\nu}M_{\mu\nu}^2-\frac{1}{\beta A}\ln\left[2e^{-\frac{\beta A}{2}\sum_\mu Q_{\mu\mu}}\sum_\mu e^{\frac{3}{2}\beta A Q_{\mu\mu}}\cosh\left(\beta B M_{\mu\mu}\right)\right], \quad (4.12)$$

which is independent of N. Introducing the reduced parameters $t = 1/(\beta A)$ and $b = B/A$, the free-energy density functional becomes

$$\mathcal{F}(Q_{\mu\nu},M_{\mu\nu}) = \frac{1}{2}\sum_{\mu,\nu}Q_{\mu\nu}^2+\frac{b}{2}\sum_{\mu,\nu}M_{\mu\nu}^2-t\ln\left[2e^{-\frac{1}{2t}\sum_\mu Q_{\mu\mu}}\sum_\mu e^{\frac{3}{2t}Q_{\mu\mu}}\cosh\left(\frac{b}{t}M_{\mu\mu}\right)\right]. \quad (4.13)$$

4.2.2 Phase Diagram

In order to make connections with experimental result, the following parametrization is introduced: $Q_{zz} \equiv S$; $Q_{yy} \equiv -S/2$; $Q_{xx} \equiv -S/2$; $M_{xx} \equiv M_{yy} \equiv 0$; and finally, $M_{zz} \equiv m$. With this choice, equation 4.13 can be rewritten as

$$\mathcal{F}(t,b,S,m) = \frac{3}{4}S^2+\frac{b}{2}m^2-t\ln\left[2e^{-\frac{3}{4t}S}\left(2+e^{\frac{9}{4t}S}\cosh\frac{bm}{t}\right)\right]. \quad (4.14)$$

The equilibrium values of the order parameters are obtained by minimizing $\mathcal{F}$ with respect to S and m in the t–b plane. Such equilibrium values are solutions of the following equations of state:

$$m = \frac{1}{3}(1+2S)\tanh\frac{b\,m}{t} \quad (4.15)$$

and

$$S = 1-\frac{3}{2+e^{\frac{9S}{4t}}\cosh\frac{b\,m}{t}}. \quad (4.16)$$

The physical meaning of the parameter b is worth emphasizing. As defined above, b controls the relative strength of the polar and nematic couplings. For small values of b, polar ordering is energetically weak, and the system reduces to the standard Maier–Saupe model. As b increases, polar interactions become more significant, leading to the stabilization of a ferronematic phase and the emergence of additional transition lines.

The factor $(1+2S)/3$ in equation 4.15 can be interpreted as the effective fraction of molecules aligned along the z-axis (the director). In the isotropic limit, $S = 0$, this factor reduces to $1/3$, recovering the orientationally averaged result $m = \frac{1}{3}\tanh(bm/t)$. In contrast, for perfect nematic order ($S = 1$), the factor becomes unity, yielding the standard Ising–Weiss equation.

The phase diagram shown in Figure 4.2 displays three distinct regions: the isotropic phase (I), the nematic phase (N), characterized by $S \neq 0$ and $m = 0$, and the ferronematic phase (N_F), for which both $S \neq 0$ and $m \neq 0$. The boundary between the N and N_F phase exist only for a finite range of the parameter b. In this region, the transition between the two phases is weak first-order—as demonstrated bellow. Beyond the indicated triple point (TP), at which $t_{TP} = 0.819$ and $b_{TP} = 1.125$, this transition disappears, and a strong first-order phase transition between the ferronematic and isotropic phases suppresses the intermediate nematic structure. Additionally, for low values of b, the nematic–isotropic transition is also of first order as expected. The field Φ in figure 4.2 is defined as $\Phi = (S + m)/2$.

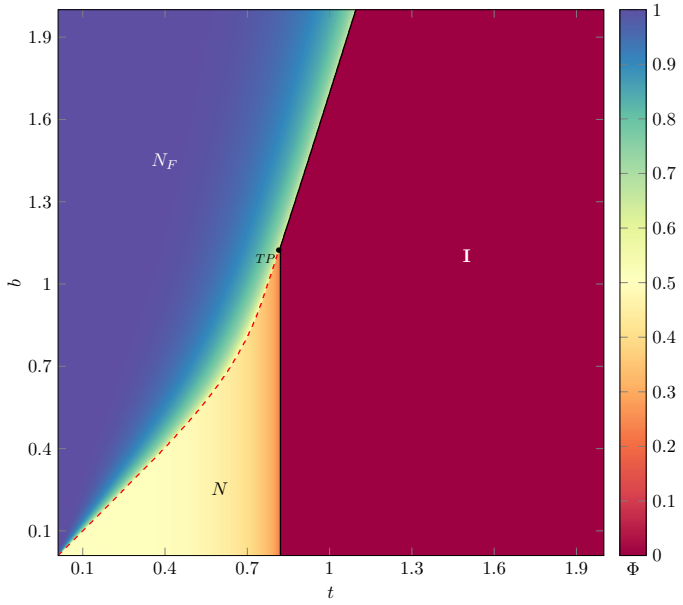

Figure 4.2: *Phase diagram for the ferronematic Maier–Saupe model in the t–b plane. The field Φ denotes the coupling between nematic and ferronematic ordering. The red dashed line indicates the weak first-order transition separating the N_F and N phases, while the solid black line corresponds to the first-order transition between ordered and disordered phases.*

The nature of the phase transitions observed in Figure 4.2 is determined by analyzing the behavior of the order parameters obtained from the global minima of equation 4.14, as well as the free energy behavior near the transition temperature. Strong first-order transitions is characterized by a discontinuity in the first derivative of the Helmholtz free energy, accompanied by a jump in the order parameter. A second-order transition, on the other hand, is characterized by a continuous vanishing of the order parameter, while the polar susceptibility χ_m—obtained by evaluating the Schur complement of the coupled susceptibility tensor (HOWCZAK and SPALEK (2010))—diverges.

In the case of a weak first-order transition, the spinodal curves lie very close to the transition temperature. This proximity results in a narrow coexistence region and a correspondingly large correlation length. As a consequence, close to the transition, hysteresis effects become difficult to resolve numerically. Under such conditions, numerical minimization procedures may follow a metastable branch, causing the transition to appear continuous and thus mimicking second-order behavior due to numerical instabilities. In this case, the polar susceptibility χ_m should exhibit a large but finite peak at the transition temperature.

To determine the nature of the transition between the ferronematic (N_F) and nematic (N) phases, both the Helmholtz free energy and the relevant order parameters must be examined. The difficulty in doing so arises from the challenge of numerically distinguishing between weak first-order and genuinely second order phase transitions. As shown in Fig. 4.3(a), the dipolar order parameter m exhibits a small discontinuity at the transition, while the discontinuity in the nematic order parameter is clear. There is also a small jump in the S order parameter in the N_F–N phase transition that can not be observed in the diagram. Furthermore, Fig. 4.3(b) shows that the Helmholtz free energy branches cross at a temperature indicated by the vertical dotted line. The simultaneous presence of a discontinuous order parameter and a free-energy crossing provides strong evidence that the $N_F - N$ transition is weakly first order. On the other hand, at the triple point, which occurs at $t \approx 0.819$ and $b = 1.125$, the three free-energy curves intersect, as shown in Fig. 4.4, indicating a change in the nature of the phase transition.

This distinction between phases is particularly important in regions where the nematic-isotropic transition approaches the ferronematic-nematic transition. For intermediate b, the system lies near a regime of phase boundary competition between the N_F and N phases. As the weak first-order transition associated with m approaches the first-order transition in S, the free energy has two close competing minima, as illustrated in Fig. 4.5a. In this regime, fluctuations on both nematic and dipolar order parameters become strongly coupled and the system undergoes a change in the nature of the phase transition. As the dipolar order parameter m

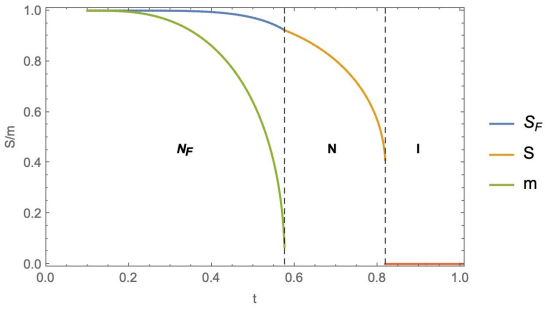

(a) *Temperature dependence of the order parameters. The N_F and N regions indicate the ferronematic and nematic phases, while the I region corresponds to the high-temperature isotropic phase.*

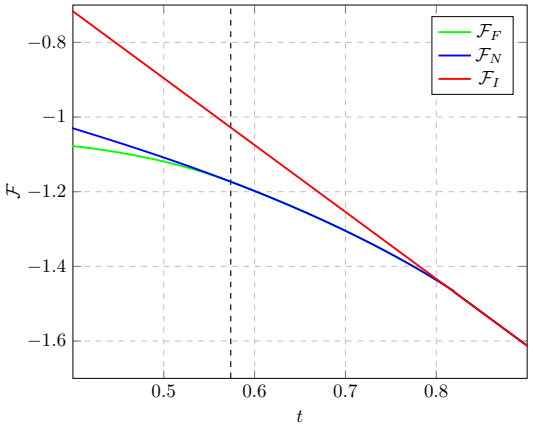

(b) *Helmholtz free energy as a function of t. The crossing of the free-energy branches signals a first-order transition.*

Figure 4.3: *Order-parameter behavior and Helmholtz free energy across the ferronematic–nematic transition for $b = 0.608$.*

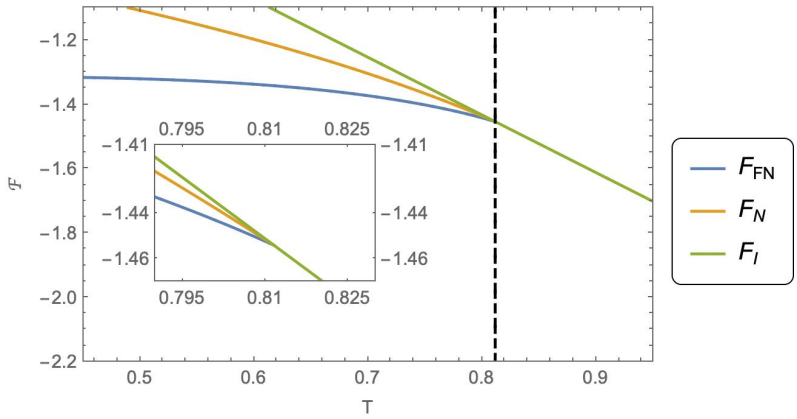

Figure 4.4: *Helmholtz free energy as a function of temperature for $b = 1.125$. The three curves are for the Nematic ($\mathcal{F}_N$), Ferronematic ($\mathcal{F}_{FN}$) and Isotropic ($\mathcal{F}_I$) phase, respectively.*

approaches zero, the coupling between dipolar and nematic degrees of freedom is progressively weakened, leading to a modification of the effective coefficient of S in equation 4.14 which is heavily dependent on m. As a result, the equilibrium value of S shifts. It is possible to see the collapsing behavior of the free energy as $m \to 0$ in Figure 4.5b. This results in a sudden change in the free energy landscape, resulting in a change in the location of the global minima.

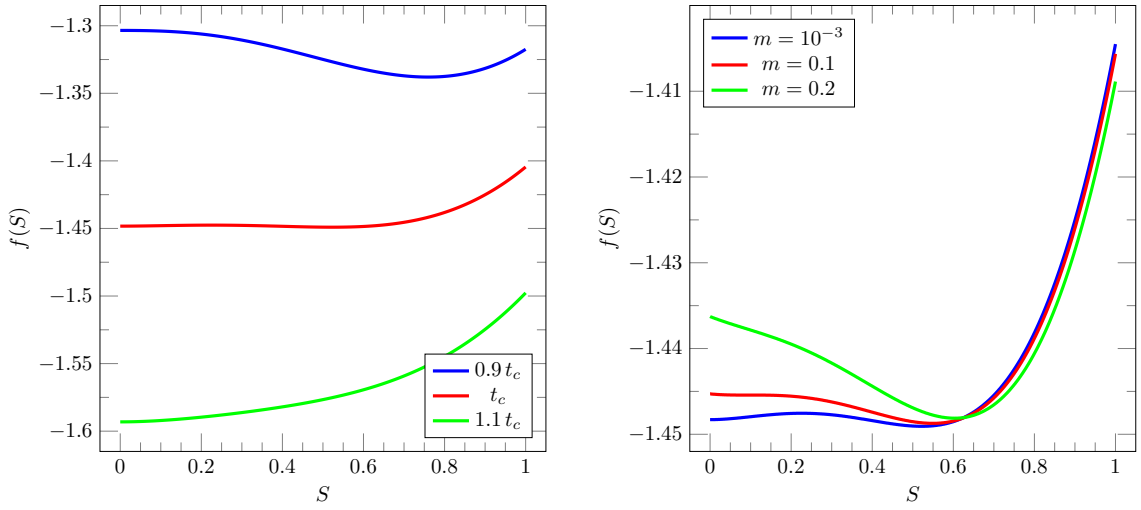

(a) *Free Energy in term of S.* ***(b)*** *Free Energy collapsing for $m \to 0$.*

Figure 4.5: *Free Energy behavior near the triple point ($b = 1.1$).*

A complete Landau–de Gennes expansion of the free-energy functional $\mathcal{F}(S, m)$ in the vicinity of the N_F–N transition line is deferred to future work. Such an analysis would, in principle, allow for a more detailed characterization of the critical behavior and the possible emergence of multicritical points. However, the main technical difficulty lies in the intrinsic coupling between the nematic (S) and polar (m) order parameters, which significantly complicates the structure of the expansion and the identification of the relevant invariants. A systematic treatment of this coupled-order-parameter problem is therefore left for subsequent investigation.

CHAPTER 5

CONCLUSIONS AND PERSPECTIVES

This thesis set out to investigate phase transitions and symmetry breaking in different liquid crystal systems. Within the framework of a mean–field theory, two extensions of the standard Maier–Saupe model were developed in order to study structural changes in thermotropic liquid crystals phases. Connections with experimental results were established introducing appropriate choices of the order parameter and through systematic expansions on the free-energy functional via Landau–de Gennes formalism.

After an introductory chapter in which the Maier–Saupe model was solved using standard methods of statistical physics, dilution effects were introduced in Chapter 3 in order to investigate the critical-like behavior of the nematic-isotropic (NI) phase transition. Within the mean-field approximation, the free-energy functional was formulated in terms of the nematic scalar order parameter S and the chemical potential $\tilde{\mu}$ associated with the occupation variable. This formulation allows for the derivation of the equations of state, from which the phase behavior of the system can be determined.

In the phase diagram defined on the $t-\tilde{\mu}$ plane a strong first order phase transition is observed, with well-defined spinodal lines. As $\tilde{\mu}$ gets close to zero, the spinodal region moves closer to the critical temperature, signaling a change in the nature of the phase transition toward a weak first-order regime. This behavior provides a theoretical justification for the emergence of a pseudo-tricritical point reported in experimental results. Moreover, a Landau–de Gennes expansion of the free energy yields an effective tricritical exponent $\beta_c = 1/3$, which is in qualitative agreement with the quasi-tricritical exponent reported by LENART *et al.* (2012) for the $E7$ compound. By introducing a new variable g, related to the inverse exponential of the chemical potential and temperature, a phase diagram on the t–g plane was constructed, offering a clear visualization of the phase behavior. In this representation, the presence of a tricritical point in the vicinity of the NI phase transition becomes evident.

In consonance with the recent discovery of the ferronematic phase, a second model was introduced to study liquid-crystal materials with nonzero molecular dipole moment, preceded by a brief review of the experimental and theoretical literature. By incorporating an additional term accounting for dipolar interactions into the Maier–Saupe framework, a rich phase diagram emerges, including the stabilization of a ferronematic phase (N_F).

The existence and stability of this phase are controlled by the parameter b, which rules the relative strength of the polar and nematic couplings. The nature of the phase transitions in the t–b plane was characterized through a combined analysis on the respective order parameter and the behavior of the Helmholtz free-energy functional. In particular, the transition between the ferronematic and nematic phase was found to be of weak-first order, a result that is qualitatively in line with available experimental observations. Despite the simplicity of this model extension, it captures the essential features of the observed phase behavior. Future work focusing on the Landau–de Gennes framework aims at determining critical exponents in the vicinity of the triple point associated with the N_F–N phase transition, with the goal of establishing more quantitative connections with experimental data.

The two model extensions proposed on this thesis highlight the versatility of mean-field approaches in capturing symmetry breaking and ordering in liquid-crystal systems. By introducing additional degrees of freedom, the Maier–Saupe framework shows itself capable of accommodating a variety of phase behaviors. Moreover, this work illustrates how the Landau-de Gennes expansion can be used to understand complex phenomena as the tricritical-like behavior of the N–I phase transition.

REFERENCES

AHARONY, A., 1982. "Lecture notes in Multicritical Points". January.

AHARONY, A., 1978, "Tricritical points in systems with random fields", *Physical Review B*, v. 18, n. 7, pp. 3318.

ANDRIENKO, D., 2018, "Introduction to liquid crystals", *Journal of Molecular Liquids*, v. 267, pp. 520–541.

BLINOV, L. M., 2010, *Structure and properties of liquid crystals*, v. 123. Berlin, Germany, Springer Science & Business Media.

CALLEN, H. B., 1993, "Thermodynamics and an Introduction to Thermostatistics", *John Wiley& Sons*, v. 2.

CHEN, R. H., 2011, *Liquid crystal displays: fundamental physics and technology*. Hoboken, New Jersey, John Wiley & Sons.

CHEN, X., 2024, "The ferroelectric nematic realm", *Liquid Crystals Today*, v. 33, n. 3, pp. 50–65.

CHEN, X., KORBLOVA, E., DONG, D., et al., 2020, "First-principles experimental demonstration of ferroelectricity in a thermotropic nematic liquid crystal: Polar domains and striking electro-optics", *Proceedings of the National Academy of Sciences*, v. 117, n. 25, pp. 14021–14031.

CRUICKSHANK, E., 2024, "The emergence of a polar nematic phase: A chemist's insight into the ferroelectric nematic phase", *ChemPlusChem*, v. 89, n. 5, pp. e202300726.

DE GENNES, P.-G., PROST, J., 1993, *The physics of liquid crystals*. 2 ed. Paris, Oxford university press.

DE OLIVEIRA, M., NETO, A. F., 1986, "Reentrant isotropic-nematic transition in lyotropic liquid crystals", *Physical Review A*, v. 34, n. 4, pp. 3481.

DIERKING, I., 2025, "Liquid Crystal Research and Novel Applications in the 21st Century", *Crystals*, v. 15, n. 4, pp. 321.

DO CARMO, E., LIARTE, D. B., SALINAS, S., 2010, "Statistical models of mixtures with a biaxial nematic phase", *Physical Review E—Statistical, Nonlinear, and Soft Matter Physics*, v. 81, n. 6, pp. 062701.

ETXEBARRIA, J., FOLCIA, C., ORTEGA, J., 2022, "Generalization of the Maier-Saupe theory to the ferroelectric nematic phase", *Liquid Crystals*, v. 49, n. 13, pp. 1719–1724.

FRENKEL, D., EPPENGA, R., 1982, "Monte Carlo study of the isotropic-nematic transition in a fluid of thin hard disks", *Physical review letters*, v. 49, n. 15, pp. 1089.

GRAMSBERGEN, E. F., LONGA, L., DE JEU, W. H., 1986, "Landau theory of the nematic-isotropic phase transition", *Physics Reports*, v. 135, n. 4, pp. 195–257.

HELFRICH, W., 1969, "Conduction-induced alignment of nematic liquid crystals: basic model and stability considerations", *The Journal of chemical physics*, v. 51, n. 9, pp. 4092–4105.

HOWCZAK, O., SPALEK, J., 2010, "Magnetoelectric correlations in BiMnO _3 whithin Landau theory: comparison with experiment", *arXiv preprint arXiv:1001.2224*.

KEYES, P., SHANE, J., 1979, "Tricritical exponents for the isotropic-nematic transition: an experimental verification", *Physical Review Letters*, v. 42, n. 11, pp. 722.

KIM, K.-H., SONG, J.-K., 2009, "Technical evolution of liquid crystal displays", *NPG Asia materials*, v. 1, n. 1, pp. 29–36.

LANDAU, L. D., 1965, *Collected papers of LD Landau*. New York, Pergamon.

LANDAU, L. D., LIFSHITZ, E. M., LIFSHITZ, L., et al., 1980, *Statistical physics: theory of the condensed state*, v. 9. Oxford,, Butterworth-Heinemann.

LEE, T.-D., YANG, C.-N., 1952, "Statistical theory of equations of state and phase transitions. II. Lattice gas and Ising model", *Physical Review*, v. 87, n. 3, pp. 410–419.

LENART, V., GÓMEZ, S., BECHTOLD, I., et al., 2012, "Tricritical-like behavior of the nonlinear optical refraction at the nematic-isotropic transition in the E7 thermotropic liquid crystal", *The European Physical Journal E*, v. 35, n. 1, pp. 4.

MAIER, W., SAUPE, A., 1958a, "Eine einfache molekulare Theorie des nematischen kristallflüssigen Zustandes", *Zeitschrift für Naturforschung A*, v. 13, n. 7, pp. 564–566. doi: 10.1515/zna-1958-0716.

MAIER, W., SAUPE, A., 1958b, "Eine einfache molekulare Theorie des nematischen kristallinflüssigen Zustandes", *Zeitschrift für Naturforschung A*, v. 13, n. 7, pp. 564–566.

MAIER, W., SAUPE, A., 1959, "Eine einfache molekular-statistische Theorie der nematischen kristallflüssigen Phase. Teil II", *Zeitschrift für Naturforschung A*, v. 14, n. 10, pp. 882–889. doi: 10.1515/zna-1959-1005.

MAIER, W., SAUPE, A., 1960, "Eine einfache molekular-statistische Theorie der nematischen kristallflüssigen Phase. Teil III", *Zeitschrift für Naturforschung A*, v. 15, n. 4, pp. 287–292. doi: 10.1515/zna-1960-0401.

MARRO, J., LABARTA, A., TEJADA, J., 1986, "Critical behavior of Ising models with static site dilution", *Physical Review B*, v. 34, n. 1, pp. 347.

MERTELJ, A., CMOK, L., SEBASTIÁN, N., et al., 2018, "Splay nematic phase", *Physical Review X*, v. 8, n. 4, pp. 041025.

METROPOLIS, N., ROSENBLUTH, A. W., ROSENBLUTH, M. N., et al., 1953, "Equation of state calculations by fast computing machines", *The journal of chemical physics*, v. 21, n. 6, pp. 1087–1092.

MUKHERJEE, P. K., 1998, "The puzzle of the nematic-isotropic phase transition", *Journal of Physics: Condensed Matter*, v. 10, n. 41, pp. 9191.

NISHIKAWA, H., SHIROSHITA, K., HIGUCHI, H., et al., 2017, "A fluid liquid-crystal material with highly polar order", *Advanced materials*, v. 29, n. 43, pp. 1702354.

NISS, M., 2005, "History of the Lenz-Ising model 1920–1950: from ferromagnetic to cooperative phenomena", *Archive for history of exact sciences*, v. 59, n. 3, pp. 267–318.

RODRIGUES, D. D., VIEIRA, A. P., SALINAS, S. R., 2020, "Magnetic field and dilution effects on the phase diagrams of simple statistical models for nematic biaxial systems", *Crystals*, v. 10, n. 8, pp. 632.

SALINAS, S. R., 1997, *Introdução a física estatística*, v. 9. São Paulo, Edusp.

SIMEAO, D., SIMOES, M., 2013, "Global order parameter critical exponent: a different calculation approach", *Molecular Crystals and Liquid Crystals*, v. 576, n. 1, pp. 88–97.

SIMOES, M., DA SILVA, J. C., 2011, "Geometrical content of Leslie coefficients", *Physical Review E—Statistical, Nonlinear, and Soft Matter Physics*, v. 83, n. 5, pp. 051702.

SIMÕES, M., SIMEÃO, D., DOMICIANO, S., 2013, "Universal nature of the nematic phase", *Molecular Crystals and Liquid Crystals*, v. 576, n. 1, pp. 76–87.

TUBIANA, L., ALEXANDER, G. P., BARBENSI, A., et al., 2024, "Topology in soft and biological matter", *Physics reports*, v. 1075, pp. 1–137.

WALLACE, W. A., 1996, *The modeling of nature: Philosophy of science and philosophy of nature in synthesis*. Washington, D.C, CUA Press.

WANG, Z., KEYES, P., 1996, "Critical and multicritical fluctuations of nematic liquid crystals", *Physical Review E*, v. 54, n. 5, pp. 5249.

WILSON, M. R., YU, G., POTTER, T. D., et al., 2022, "Molecular simulation approaches to the study of thermotropic and lyotropic liquid crystals", *Crystals*, v. 12, n. 5, pp. 685.

YEOMANS, J. M., 1992, *Statistical mechanics of phase transitions*. Oxford, Clarendon Press.

ZWANZIG, R., 1963, "First-order phase transition in a gas of long thin rods", *The Journal of Chemical Physics*, v. 39, n. 7, pp. 1714–1721.